Copyright Warning & Restrictions

The copyright law of the United States (Title 17, United States Code) governs the making of photocopies or other reproductions of copyrighted material.

Under certain conditions specified in the law, libraries and archives are authorized to furnish a photocopy or other reproduction. One of these specified conditions is that the photocopy or reproduction is not to be "used for any purpose other than private study, scholarship, or research." If a, user makes a request for, or later uses, a photocopy or reproduction for purposes in excess of "fair use" that user may be liable for copyright infringement,

This institution reserves the right to refuse to accept a copying order if, in its judgment, fulfillment of the order would involve violation of copyright law.

Please Note: The author retains the copyright while the New Jersey Institute of Technology reserves the right to distribute this thesis or dissertation

Printing note: If you do not wish to print this page, then select "Pages from: first page # to: last page #" on the print dialog screen

ABSTRACT

EFFECT OF TURBOSTRATIC ORIENTATIONS AND CONFINED FLUID ON MECHANICAL STRENGTH OF BI-LAYER GRAPHENE: A MOLECULAR DYNAMICS STUDY

by
Nil Bharatbhai Dhankecha

The rise of graphene as a reinforcement material in the last decade has been exponential owing to its superior mechanical properties. This one atom thick 2D material is applicable in many industries related to nanomechanical, nanoelectronics and optical devices. Despite its strength and superior properties, single-layer graphene tends to be unstable in a free-standing form. This led to active use of bi-layer and multilayered graphene in many of the above-stated applications. Though properties of single-layer graphene have been extensively investigated both computationally as well as experimentally for over a decade, bilayer graphene and its turbostratic form are still under research. Additionally, little is known about the effects of environmental condition such as humidity on the mechanical strength of these layered structures. Therefore, the detailed investigation of these bi-layered structures and their derivatives for real-life applications is crucial.

In this study, the mechanical properties of these structures are investigated by means of Molecular Dynamics (MD) simulation. MD simulations provide a cost-effective tool to study physical and chemical interaction of atoms in such structures. Simulations have proved to be very efficient in modeling structures and predicting their mechanical properties. Herein, single-layer graphene, bilayer graphene were exposed to uniaxial tensile load in zig-zag and armchair direction. Different turbostratic orientations of

bilayer graphene were also subjected to uniaxial loading in order to determine the most stable and strong bi-layer conformation. It was found that AB stacked bilayer graphene was most stable and was reported to have the highest strength of all other bilayer conformations. For further bi-layer analysis, AB stacking was preferred. The analysis was further extended to study crack propagation in single and bilayer graphene. The study was completed by understanding the effect of fluids such as water confined in bilayer graphene on its overall mechanical strength. In the past decade, several applications have come to light ranging from sensors to biomedical devices that employ such constructed nano-structures. However, the question of the mechanical stability of such structures with different water content is rarely addressed. Herein, the effect of fluid confined in bilayer graphene on its mechanical property was detailed. The results show an increased strain limit in the graphene in the presence of water content and provide an interesting insight into the surface hydrophobicity of graphene.

EFFECT OF TURBOSTRATIC ORIENTATIONS AND CONFINED FLUID ON MECHANICAL STRENGTH OF BI-LAYER GRAPHENE: A MOLECULAR DYNAMICS STUDY

by
Nil B. Dhankecha

A Thesis
Submitted to the Faculty of
New Jersey Institute of Technology
in Partial Fulfillment of the Requirements for the Degree of
Master of Science in Mechanical Engineering

Department of Mechanical and Industrial Engineering

August 2019

Dedicated to

My Family

APPROVAL PAGE

EFFECT OF TURBOSTRATIC ORIENTATIONS AND CONFINED FLUID ON MECHANICAL STRENGTH OF BI-LAYER GRAPHENE: A MOLECULAR DYNAMICS STUDY

Nil B. Dhankecha

Dr. Dibakar Datta, Dissertation Advisor — Date
Assistant Professor of Mechanical Engineering, NJIT

Dr. Pushpenra Singh, Committee Member — Date
Professor of Mechanical Engineering, NJIT

Dr. Zhiming Ji, Committee Member — Date
Professor of Mechanical Engineering, NJIT

BIOGRAPHICAL SKETCH

Author: Nil B. Dhankecha

Degree: Master of Science

Date: August 2019

Undergraduate and Graduate Education:

- Master of Science in Mechanical Engineering,
  New Jersey Institute of Technology. Newark, NJ

- Bachelor of Science in Mechanical Engineering,
  Marwadi Education Foundation Group of institutes. Rajkot, Gujarat India. 2017

Major: Mechanical Engineering.

ACKNOWLEDGMENT

I would like to thank Dr. Dibakar Datta for this great opportunity. Knowing that I am new to this field and giving me time to understand the basics. This project has been a very good learning experience under his guidance. Without his continuous guidance and support, this work could not have been completed. I will always be grateful for this opportunity and constant inspiration.

I would also like to thank Dr. Zhiming Ji and Dr. Pushpenra Singh for serving in my committee. Their suggestions have been valuable for improvement in my report and results. I will always be grateful to Dr. Zhiming Ji for his guidance as an academic advisor. It helped me very much to complete my project on time.

Thank you, Ms. Vidushi Sharma and Mr. Jatin Kashyap, my mentor and lab mates for their continues support and guidance. You taught me how research is being done and other aspects of it. I would also thank Dr. Kamalika Ghatak for all the wonderful conversations throughout the year.

Finally, I would never be able to thank my parents enough for all the love and support because of whom I am in the United States of America. Also, My Uncle and Aunt who are like my second parent, have the same contribution in my success. I would also thank my roommates for encouraging and supporting me all this time.

TABLE OF CONTENTS

TABLE OF CONTENTS
(Continued)

LIST OF FIGURES

LIST OF FIGURES
(continued)

LIST OF FIGURES
(continued)

LIST OF TABLES

CHAPTER 1

INTRODUCTION

1.1 Overview

Ever since the discovery of graphene, the strongest material in the world, researchers are trying to incorporate graphene to enhance technology in every possible way. Due to its exceptional quality, it has the potential to be used in a variety of applications. Bioelectric sensing device, organic light-emitting diodes, photovoltaic cells, energy storage devices, composite material to name a few [1-3]. Graphene offers exceptionally high tensile strength, large surface area, high electrical and thermal conductivity. It is 40 times stronger than diamond and 300 times strong then A36 structural steel[4]. Although the synthesis of graphene is still a challenge in the scientific community, there are no reliable means of large-scale production of graphene with low cost. In 2004 Andrei Geim and Kostya Novoselov accidentally found a way to mechanical exfoliate graphene from graphite with help of a scotch tape[5]. In the last decade new techniques have been used successfully to develop graphene such as 1) mechanical exfoliation 2) chemical reduction 3) chemical vapor deposition (CVD) and recently found 4) plasma-assisted chemical vapor depositions (PECVD). However, single-layer graphene is often used with a substrate graphene sheet depending on applications and functionality. Also, often working environment plays a very crucial role in behavior and the properties of bilayer graphene. Applications like strain sensors and optical sensors often work in a moist area. This condition exposes graphene to some or more amount of water molecule. The mechanical properties of bilayer graphene

and its behavior under tensile load is of great interest of research. In this study, the properties and behavior of such structures have been investigated.

Molecular Dynamics simulation is a tool to mimic the behavior of such material. In this study, MD simulation is used to find mechanical properties of graphene and its bilayer variations under tensile load. The details and procedure are explained in upcoming chapters.

1.2 Objective and Scope

This study focuses on the investigation of the properties of bilayer graphene and its turbostratic variations. Following objectives will be investigated.

a) Mechanical properties of bilayer graphene.
b) Crack propagation of single and bilayer graphene.
c) The effect of a substrate graphene layer on its mechanical properties and crack propagation.
d) Stability and mechanical properties of turbostratically oriented bilayer graphenes.
e) Mechanical properties of water confined bilayer graphene.
f) Effect of the inter-layer space (slit width) on mechanical properties of water confined bilayer graphene
g) The behavior of bilayer graphene with confined water molecules.
h) Study of motion of water molecules confined in graphene.

Due to a defect in CVD synthesized graphene microscopic water droplets are present in graphene. This cause change in its desired function. This study tries to investigate the

change in the mechanical properties to predict and compensate for the error in the functioning of nanocomposite material reinforced with bilayer graphene.

CHAPTER 2

LITERATURE REVIEW

Ever since the first discovery of graphene's exceptional mechanical properties[6], it has been a subject of keen research among the scientific community. There are limitless possibilities of its application in nanotechnology, biomedical science, communication field[7]. Researchers are exploring the use of graphene reinforced material in our everyday life and this graphene reinforced material can change the way we use technology to make vehicles, buildings, and aviation. Since single-layer graphene in a stable form is near to impossible to achieve, the scientific community is trying to use the graphene in the bilayer or flake form as a reinforcement material to enhance the strength and efficiency of today's technology[8]. This advancement could be of any field, be it efficient conductor in a smartphone, an optical sensor or bulletproof vests [9]. Graphene doped polymer can also be synthesized and used extensively.

Due to its size limitation and complexity of manufacturing synthetic graphene in a laboratory, researchers have used Molecular dynamics approach to investigate mechanical, chemical and electrical properties of this material. With the help of new and improved computation techniques of MD simulation, it has become a very wide area of research. Some of the work done previously has been detailed in the following sections.

2.1 Single-layer Graphene Sheet

2.1.1 Experimental Studies

The single-layer graphene was discovered in 2004[5] and it was experimentally synthesized by the means of CVD (Chemical Vapor Depositions) in 2009[10]. This graphene showed the same mechanical and electronic properties as mechanically exfoliated graphene. Geim at al.[11] have explored the areas of science that can be revolutionized by this discovery of a material that is only one atom thick and has a carbon honeycomb structure. Experiments have shown a sheet of one atom thickness can be stable under ambient conditions. They have high crystal quality and are continues at microscopic scale[12]. This indicated that in specific conditions, a perfect graphene structure can be synthesized. These atomically perfect graphene structures are very strong in nature. Lee at al. performed nanoindentation to investigate the mechanical properties of graphene using an atomic force microscope. Their study measured the breaking strength of 42 N m^{-1}, the intrinsic strength was measured around 130 GPa and. The Young's Modulus of such material was recorded at E = 1.0 TPa experimentally[6]. This study was further extended by Zhang at al[13] where fracture toughness was tested experimentally using nanomechanical devices. They used Griffith's theory to determine the fracture toughness of graphene. The fracture toughness was measured in the form of a critical stress intensity factor.

2.1.2 Computation Studies

Molecular dynamics simulation is an advanced technique which provides alternative means to study such materials where otherwise advance laboratory setups are required. Single-layer graphene has been extensively studied by means of MD simulations. Min and Aluru[14] used the MD approach to investigate the shear strength on zig-zag graphene. The shear stress value at the edge of graphene was measured at 97.5 GPa. The effects of temperature and the free edge on the fracture of graphene was investigated using molecular dynamics using AIREBO potential by Dewapriya [15]. Their results showed that fracture toughness of graphene decreases with increase in temperature. Also, Zig-zag graphene's Young's modulus and tensile strength are highly affected by a free surface. However, for armchair graphene, the influence of free surface was comparatively less. Predicting the fracture of graphene is done by analyzing its stress intensity factor and J integral values. Jia-sin at al.[16] also found the stress intensity factor with Hardy stress formulation method and the results were in agreement with previous methods. Xu at al.[17] investigated the stress intensity factor of zig-zag and armchair graphene. They found that post-fracture, the crack propagation in zig-zag graphene was self-similar while in armchair graphene it was irregular. The critical stress intensity factor in zig-zag and armchair graphene was found to be 4.21 Map/m and 3.71 Mpa/m respectively. Datta at al.[18] extended the study to investigate the mix mode loading effects on the crack propagation effects and on the fracture strength. The study also found that armchair graphene offers more resistance during fracture of pre-cracked graphene. Recent studies have investigated the effects of defects and crack length on the fracture strength of the graphene. Xiujin at al.[9] investigated that the crack propagation speed is highly dependent on material values. It

showed the nominal plastic zone around crack tip under critical stress varies with 2D lattice. The study of single-layer graphene sheet has been extensively done over the last decade since its discovery.

The crack propagation in single-layer graphene is also studied as mentioned above but the effects of a substrate layer in the crack propagation have not been investigated. Bilayer graphene has enormous potential due to its electrical properties. Previous work done in bilayer graphene is discussed in the next chapter.

2.2 Bi-Layer Graphene Sheet

Graphene is only a single atom width 2D material. Multiple graphene sheets form graphite which is not as strong as graphene due to sliding in between the layers[19]. While bilayer graphene is made of two single-layer graphenes stacked with AA orientation. Bilayer graphene is relatively less studied than single-layer graphene. But when it comes to graphene-based nanocomposite materials bilayer graphene is the generally used material. Experiments have shown that the majority of nanocomposite where graphene has been used as reinforcement to enhance its mechanical or electrical properties have bilayer graphene rather than single-layer graphene[20, 21]. Bilayer graphene has the potential to become an alternative to silicon used in semiconductors [22]. These graphene semiconductors can be smaller than silicon semiconductor. Lin at al[23] investigated a transistor made from single-layer graphene faces interface problems while bilayer stacking can reduce the problem. Bilayer graphene also exhibits unusual optical properties. Huang et al.[24] studied spectroscopic features of single-layer and bilayer graphene. It showed that inter-

Landau-level absorption spectrum in bilayer graphene was higher than the single-layer graphene. Moreover, bilayer graphene also has potential applications due to its electronic properties, It can be used for switching functions in nonelectrical devices [25]. These properties have been extensively studied. However mechanical properties of bilayer graphene and bilayer graphene with turbostratic orientation are still a subject of research. bilayer graphene has variation based on stacking patterns. Jeong et al.[26] demonstrated a method to visualize AA stacked(bilayer) and AB stacked(Bernal) graphene. Electronic structure and electric bond structure of Bernal stacking have also been studied [27]. AB stacking is found to be more stable because half of the carbon atoms sit on the carbon in the lower layer while half of the carbon atom sits at the center of the honeycomb structure of the lower layer. Due to this property, Bernal graphene exhibits better optical properties. Jiao et al.[28] studied the mechanical properties of the bilayer and Bernal graphene. The Young's modulus for bilayer graphene in zig-zag and armchair direction are 797.2 GPa and 727.4 GPa, while for Bernal graphene its 646.7 GPa and 603.5 GPa. Zhang et al.[29] studied the mechanical properties of bilayer graphene bonded with sp^3 bonds. The Young's modulus and intrinsic strength of bilayer graphene reduces due to sp^3 boding. While interlayer interaction and stability has gone higher. The interlayer distance reduces due to sp^3 bonding. Recently mechanical properties of bilayer graphene was investigated alongside polythene at micro and nanoscale using nanoindentation experimentally[30]. Rezania et al.[31] investigated the theoretical thermal conductivity of bilayer graphene.

Mechanical properties of bilayer graphene and its stacking variation is still a vast field of study. The effects of a crack in the bilayer and crack propagation have not been

studied yet. In this study, the crack propagation in bilayer as well as single is studied and compared.

2.3 Water Confined Graphene Sheets

Graphene water interaction has been a subject of great interest among researched for a decade now. Graphene due to its exceptional properties serves as reinforcement in numbers of materials as mentioned earlier. These chemical or biological applications are most likely to be in a place where micro water molecules are present all the time. Graphene has an ambiguous behavior in the presence of water. This behavior is dependent on numbers of variable like slit width[32], contact angle[33], temperature[34] and polarity[35], to name a few. Leenaerts et al.[36] used Density Functional Theory(DFT) to study the behavior of graphene in the presence of water. Using DFT, graphene exhibited hydrophobic behavior. These results led to other studies where graphene is utilized where water deposition was needed to be reduced[37]. Leenaerts et al. again published different results using DFT explaining contradictory behavior of graphene. According to the results, water molecules are adsorbed on the graphene surface at room temperature and cannot be desorbed at the same temperature[38]. Later it was observed that this behavior is a result of a complex combination of H bonding and van der Waals interactions[39, 40]. J. Rafiee et al.[41] analyze the wettability of graphene-coated over other materials to find how the contact angle plays an important role in wettability of graphene. Graphene's thermal conductivity is found to be very high[42]. It is observed that when adsorbed in graphene liquid laying at the interface largely impacts thermal resistance[43]. Recently water confinement between two graphene layers was investigated. The effects on water density as a function

of slit width was analyzed in the study[44]. S.A. Deshmukh et al.[32] used Molecular Dynamics simulation to study fluxional properties of water molecules confined in multiple graphene layers. modified TIP3P water model was used[45] along with the effect of slit width on the behavior of water molecule. LJ potential was used to compute the interaction between water and graphene by analyzing the density variation with slit width, hydrophobic behavior of graphene was observed. Recently effect of commensurability on the viscosity of water flowing through graphene sheets was analyzed[46]. They observed that shear viscosity of water is enhanced and have oscillation originating between commensurability of slit width. Hwang et al.[47] did conductance mapping of water interaction with graphene on mica. And observed that graphene's conductivity is decreased near the water layer edge. Recently P. Solanky, at al [48] used MD simulation to study the behavior of graphene flacks in contact with water droplet. They also studied the effect of water droplet on mechanical properties of graphene.

So far, a lot of research has been done to understand the behavior of water confined graphene. But the behavior of this interaction is still ambiguous and of keen interest among researchers. The effects percentage of water molecule's effect on the hydrophobicity is still under investigation. Graphene optical sensor uses graphene film as a coating. These sensors are required to work on a dry and wet environment. In these types of situations, the knowledge of the behavior of graphene becomes very essential. In this study, the effect of slit width and number of a water molecule on hydrophobicity and mechanical properties are analyzed.

CHAPTER 3

METHODOLOGY

3.1 Molecular Dynamics Simulations

Molecular dynamics (MD) simulations is a technique to study the atomic motion by using a simple approximation based on Newtonian physics. It is a technique for simulating physical and chemical interactions of atoms and molecules. This technique was first developed in the 1950s to overcome complexity and computational intensity of molecular dynamics computations. This method was first proposed by Ulam and Tsingou in mid-1950[49]. And was first applied by Alder and Wainwrightin 1956 [50] to simulate a collision between two spheres. In recent years advancement in the field of nanotechnology has made molecular dynamics simulations a very popular technique. It provides a bridge between macroscopic experiments in the laboratory and its microscopic study. This method predicts the static and dynamic properties of molecule by understanding and calculating the interactions between each atom in the system.

Molecular dynamics has vast applications due to its simplicity in fields of nanotechnology, material science, biotechnology, biochemistry, and biophysics to name a few. Its first application in biological processed was discovered by Warshel[51], This led to further understanding of the motions in proteins. It is also a very useful tool when it comes to analyzing the material properties of nanomaterial such as graphene. In this study mechanical properties of graphene are analyzed using MD simulations.

3.2 Molecular Dynamics Simulation Process

As mentioned in the previous section, MD is a technique for simulating physical and chemical interaction between atoms and molecule. MD process step by step solves Newton's equation of motion for each atom in the system. By updating the atom's position and energy information in every step, it predicts the movement of the atom affected by its neighbor atoms. For a system of N atoms, it solves the following equation of motion:

$$m_i x_\iota = -\frac{\partial V(\ddot{x}_1^t,\ x_2^t, \dots x_N^t)}{\partial x_\iota^t} \equiv F_i^t (i = 1,2, \dots N) \tag{3.1}$$

Where force F_i of an atom(i) whose mass is m_i and position x_i, is calculated from the user-defined potential energy(V). This process runs in a cycle to compute properties of the N-particle system.

Fig. 3.1 illustrate the process of MD simulations. Initial configuration involves an input data file containing information of initial position and velocity of atoms in the system. This data file also contains the information of mass, bond type, bond angle, charge, and dihedral depending on the type of molecular system. To simulate the system at finite temperature, initial velocities are assigned to the atoms. Then their updated position and velocities are computed using equation (3.1). Forces acting on atoms due to their interaction with other atoms are computed using the potential function. deformation, temperature and pressure condition are applied to the system to analyze its behavior under certain physical condition using ensemble. This process is done each

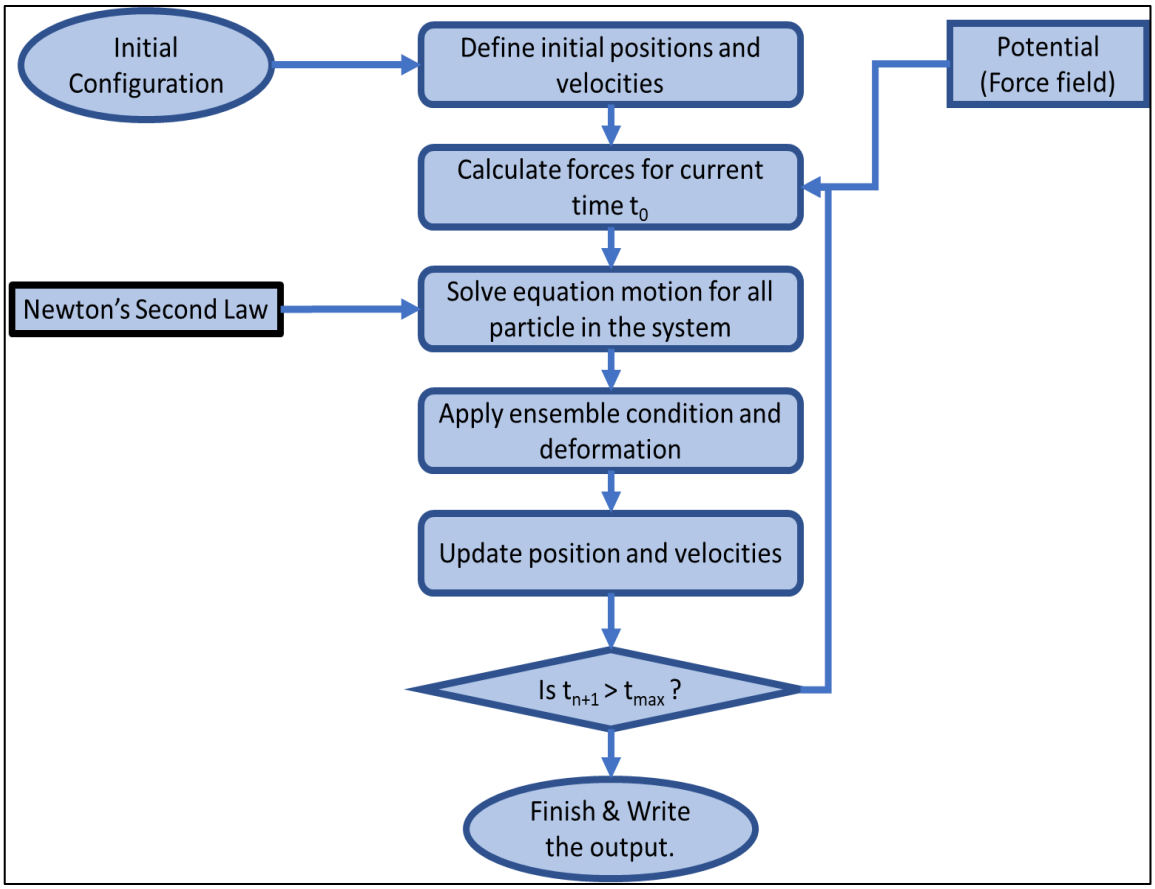

Figure 3.1 Flow chart of molecular dynamic simulations.

timestep. The value of a time step is predefined in the system. To compute the updated position and velocity of the N-particle system at each time step, various numerical integration techniques used are as follows:

1. Varlet Algorithm
2. Leap-frog Algorithm
3. Beeman's Algorithm
4. Velocity Varlet Algorithm

In this study Large-Scale Atomic/Molecular Massively Parallel Simulator (LAMMPS), open-source software has been used to perform the MD simulations. LAMMPS uses the Velocity Varlet Algorithm among the numerical integration techniques listed above to compute the velocities and positions of the atoms. The details of the simulations tools and parameters are elaborated in upcoming chapters.

3.3 MD Simulation Using LAMMPS

Large-Scale Atomic/Molecular Massively Parallel Simulator(LAMMPS) is an open-source software which performs MD simulation developed by Sandia National Laboratories. It uses Massage Passing Interface (MPI) to perform large MD calculation through parallel computing. LAMMPS uses the neighbor list to keep track of the nearby particles. For this, it uses the Velocity Varlet Algorithm which is very efficient and common numerical integration method[52]. In this method, the values of velocities and position are calculated at the same value of time variable. So, this method gives a very precise calculation of updated position and velocity with timestep. In this method, the velocities 'v' and the positions 'x' at a time 't + Δt' is given by

$$\mathrm{v}(t + \Delta t) = v(t) + \frac{1}{2}(a(t) + a(t + \Delta t))\Delta t \tag{3.2}$$

$$\mathrm{r}(t + \Delta t) = r(t) + v(t)\Delta t + \frac{1}{2}a(t)\Delta t^2 \quad (3.3)$$

LAMMPS uses the same process described in fig. 3.1. It takes a data file containing initial information of atoms position and velocities. This data file can be of different type such as atomic, molecular, full and charge depending on the types of atoms and the information stored inside. LAMMPS run on an input script which has 4 parts: 1) Initialization: Initialization defines the very basic parameters needed to define a system such as units, boundary conditions, processors, timestep and most important, a potential function. 2) Atom definition: the data file is read in this section. This data file could be initial conditions of the system to start a simulation or it could be a restart file to continue a previous simulation. LAMMPS can also create atoms on its own without any datafile. 3) Settings: this is the most import part of the simulation as all the parameter needed to be calculated can be controlled by settings. After the initial condition and environment are defined for the simulation, variety of setting can be applied to the system. This setting includes modification in potential by changing pair coefficient, bond coefficient, and angle coefficient. The size of the neighbor list and timestep can also be modified in the settings. Fixes can be defined to impose different boundary condition such as deformation. Heating or cooling of the system can be contrived by applying ensembles. The output values generated due to new boundary condition and fixes can also be calculated and stored in this section by a compute command. These values can be stress per atom, the kinetic energy of the system, potential energy of the system, temperature, densities, etc. 4) Running the simulation: when all the initial condition, timestep, fixes, and computes are defined the

simulation is run. It gives predefined output values each timestep and dumps it in the form of an output file which letter can be accessed and post processed by visualization tools.

This chapter explains how an MD simulation takes place in LAMMPS. In this process, each parameter and system definition plays a key role to make the simulation as close as possible to an experimental setup. The parameters used in this study are described in the following sections.

3.4 Thermostats

Thermostats are used in MD to control the system's temperature at a finite value. Temperature control is very important in MD simulation to obtain results close to an experimental setup. Thermostats are also a necessary input when the goal of the simulation is to study the effects of temperature fluctuation on a molecular system. According to equipartition theorem, the average internal kinetic energy (K) of the system is related to its microscopic temperature (T). The relationship between temperature and kinetic energy can be described as follows

$$\mathrm{T} = \frac{2}{3}\frac{\langle K \rangle}{N k_B} \tag{3.4}$$

Where, K_b is Boltzmann's constant, N_{df} the number of internal degrees of freedom of the system, K is the Kinetic energy of the system at t time. The thermostat only controls

the average value of the temperature throughout the simulation as it is not feasible to control the temperature at a fixed point due to fluctuations in the velocity of the atoms. As given in equation 3.4, the temperature of the molecular system only depends on the kinetic energy of the system, as the kinetic energy of the system depends on the random velocity of individual atoms. Thus, a thermostat uses velocity scaling to control the average temperature of the system. Some of the common thermostat used are discussed below.

3.4.1 Nose-Hover Thermostat

In MD simulations, the Nose Hoover thermostat is most commonly used and is referred to as the most accurate thermostat. It was developed by Nose[53] and then later improved by Hoover[54]. Nose-Hoover thermostat introduces a virtual mass to the system and links the simulated system to the virtual mass using one or more virtual chains. The temperature of the system is controlled by inserting or extracting energy to and from the simulated system using linked virtual mass. This thermostat determines the temperature adjustments by initial values.

In LAMMPS Nose-Hoover thermostat is implemented by defining a fix NVT which is discussed in the upcoming sections.

3.4.2 Berendsen Thermostat

Berendsen thermostat rescales the velocities of the particles in MD simulation to control the desired temperature of the system. Berendsen thermostat is useful due to its efficiency

with the large systems. In this thermostat, the whole system is weakly coupled to a heat bath of some temperature. In order to control the temperature of the system Berendsen thermostat suppresses the fluctuation of the kinetic energy of the system,

$$\frac{dT(t)}{dt} = \frac{1}{\tau}\,(T_0 - T(t)) \tag{3.5}$$

Where τ is the coupling parameter. The fluctuation in temperature reduces exponentially with time. The change in temperature between two successive time steps is,

$$\Delta T = \frac{\delta t}{\tau}\,(T_0 - T(t)) \tag{3.6}$$

3.5 Ensembles

Ensembles in MD simulation are used to keep the system at constant energy or at a constant temperature. An ensemble is a system which uses newton's equations to perform energy conservation. It can also add or remove heat from the system to maintain it at constant temperature or pressure. There are three ensembles available to control these parameters. These ensembles are as follows.

3.5.1 NVE Ensemble

NVE ensemble, also known as a micro-canonical ensemble is a statistical ensemble. It is used to isolate a system from its surrounding environment. The system in the presence of the NVE ensemble cannot transfer any energy or number particle with the surrounding. It keeps the energy of system constant as time goes on. As its name suggests, the microscopic variable which can affect the nature of the MD system such as the number of particles in the isolated system(N), the volume of the system(V), and the total energy(E) are constant of this ensemble.

3.5.2 NVT Ensemble

When a molecular system is coupled to an infinite heat bath, but particle exchange does not take place between the heat bath and the system, it forms a canonical ensemble. NVT is a canonical ensemble used in MD simulations. For NVT ensemble energy transfer can take place in between the system and the bath resulting fluctuation in the system's total energy. But the temperature of the system remains constant throughout the simulation. As its name suggests the number of particles(N), the volume of the system(V), and the temperature values(T) are responsible for the behavior of the system. NVT ensemble does not evolve with time because it's a function of a system's energy only.

3.5.3 NPT Ensemble

NPT is also a canonical ensemble. It is an isothermal and isobaric ensemble. The number of particles(N), pressure of the system and the temperature of the system is constant throughout the simulation. A thermostat and barostat are required to control the temperature and the pressure of the system. Nose-Hoover and Berendsen thermostat discussed above are used to control the temperature of the system. This ensemble is very efficient when the behavior of the system during the simulation is required closed to the behavior of experimentation in laboratory conditions. LAMMPS uses this ensemble by using fix NPT commands. It also gives you flexibility when it comes to controlling the pressure in targeted components only. In this study, the pressure control is only done in x and z or y and z component due to required deformation in the system. Fig 3.2 illustrates all three ensembles applied to an MD system

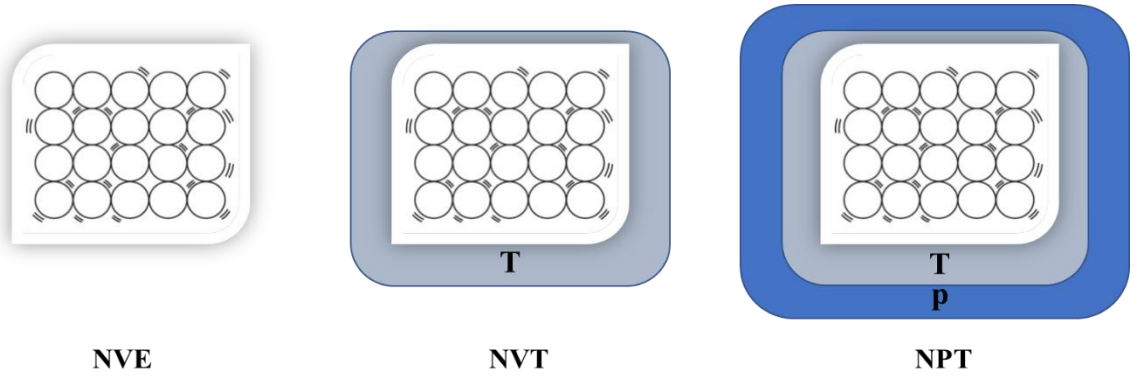

Figure 3.2 NVE, NVT and NPT ensemble applied to a MD system.

3.6 Periodic Boundary Condition

While performing MD simulation to obtain material properties of a system, the effect of surface energy must be taken into consideration. To eliminate the finiteness of the system and effects of the free surface in the system, Periodic Boundary Conditions (PBC) are used. By applying periodic boundary conditions, the primary cell shown in Fig.3.3 is replicated

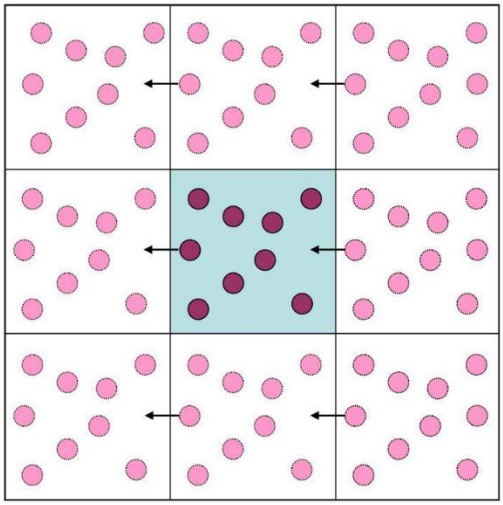

Figure 3.3 Boundary conditions applied in MD system.

Source: Gkeka, P., Molecular dynamics studies of peptide-membrane interactions: insights from coarse-grained models. 2010.

in all the 3 cartesian directions. The particle with similar position and velocity values will be replicated in those cells. The cells are arranged by a regular lattice defined by three repeat vectors: c_1, c_2, c_3. Now if there was an atom at location x_i in the primary cell. And there are n replicates of the primary cell now there will be n particle at the position of $x_i + n_1c_1 + n_2c_2 + n_3c_3$. where n_1, n_2, n_3 are constant. There is no defined boundary between the primary cell and replicated cell. The atoms in the primary cell interact within the primary cell and with the atom in the replicated cell also. In periodic boundary conditions, if an

atom exits from the cell wall, an identical atom with the same velocity and energy level will enter the same cell from the opposite side of the wall

3.7 Molecular Dynamics Potentials

The potential function has a very important role to play in the Molecular Dynamics simulations. the velocity and positions are computed form the acceleration of the particle in a molecular system. These accelerations of the particle are determined by the force field (Potential Functions). To perform MD simulations as close as possible to laboratory experiments, this potential must be defined precisely. Researchers have done very vast research to make these potentials to perform MD simulation just like experimental situations. In this study, AIREBO and LJ potential for TIP4P water model has been used to perform MD simulation. Details of these potential are as follows.

Adaptive Intermolecular Reactive Bond Order (AIREBO) potential is an improved version of REBO potential[55]. The potential was primarily developed to simulate a system of carbon/hydrogen atoms. AIREBO potential is the sum of REBO potential, the Lennard-Jones (LJ) potential, and the torsional potential.

$$\mathrm{E} = \frac{1}{2}\sum_{i}\sum_{j\neq i}\left[E_{ij}^{REBO} + E_{ij}^{LJ} + \sum_{k\neq i}\sum_{l\neq i,j,k} E_{kijl}^{TORSION}\right] \tag{3.7}$$

AIREBO potential has been extensively used to simulate graphene and its variation and it almost gives similar results as the experiments[56, 57]. In this study, AIREBO potential with an interaction cut-off of 1.92Å is taken[58]. AIREBO potential also computes van der Waals long-range interactions from LJ potential and a torsional term from the σ-bond torsion.

Non bonded interactions are defined as interaction due to attractive and repulsive forces at small atomic distances. Van der Waals interactions are the primary none-bonded interaction found in MD simulation. LJ potential is commonly used to describe these non-bonded interactions[59]. This potential is also termed as 6-12 potential or 12-6 potential. It can be written as,

$$V(r) = 4\varepsilon\left[\left(\frac{\sigma}{r}\right)^{12} - \left(\frac{\sigma}{r}\right)^{6}\right] \tag{3.8}$$

Where ε is the depth of the potential wall, σ is a finite distance where interparticle distance is zero, r is the current distance between two particles. figure 3.4 shows variation in LJ potential as a function of distance

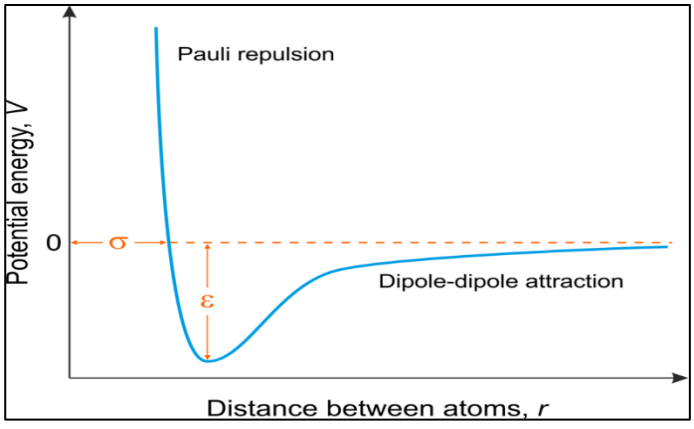

Figure 3.4 Variation in L-J potential with distance(r).

3.8 Description of MD System

3.8.1 Single and Bilayer Graphene

In this study, crack propagation in single-layer and bilayer graphene and the effect of the presence of a substrate layer on crack propagation is analyzed. As mention above this study has been done using LAMMPS software using Adaptive Intermolecular Reactive Bond Order (AIREBO) potential. Periodic boundary conditions are applied to eliminate the effects of the finiteness of the structure. The default cut-off parameter 1.92 Å for AIREBO was used throughout the simulation. The timestep for the MD simulation was 1 fs. The system was given random velocities and that were relaxed for 10 ns. The relaxation was done using the micro-canonical ensemble (NVE). Followed by relaxation, homogeneous strain was applied to the system in zig-zag as well as in armchair direction. The strain with a low strain rate of 0.001 fs^{-1} was applied by deforming the simulation box and remapping the atoms at the same time. Stress generated due to this strain in each atom ware computed in LAMMPS using virial stress theorem[60]. According to the equation,

$$\sigma_{ij}^{\gamma} = \frac{1}{\Omega^{\gamma}} \left(\frac{1}{2} m^{\gamma} v_i^{\gamma} v_j^{\gamma} + \sum_{\beta=1,n} r_{\gamma\beta}^{i} f_{\gamma\beta}^{i} \right) \tag{3.9}$$

where i and j denote indices in Cartesian coordinate systems. γ and β are the atomic indices, m^{γ} and v^{β} denote the mass and velocity of atom γ, $r_{\gamma\beta}$ is the distance between atoms γ and β, Ω^{γ} is the atomic volume of atom γ. Then the strength of the graphene sheet is calculated by averaging stress over all the carbon atoms[61]. The tensile stress is calculated

by taking the sum of all the axial component of forces on carbon atoms then dividing it by cross-section area. This method was used by Datta et al[18] To find the effect of crack length in fracture of graphene. In an extension of this method Stress Intensity factor of graphene with crack was investigated using the equation below,

$$K_I = \sigma_n \sqrt{\pi a} \tag{3.10}$$

Where K_I is mode I stress intensity factor, σ_n is stress value at the time of first bond breaking, a is the crack length. The results of these calculations are presented and discussed in chapter 4. Following structures were used to determine the MD simulation results:

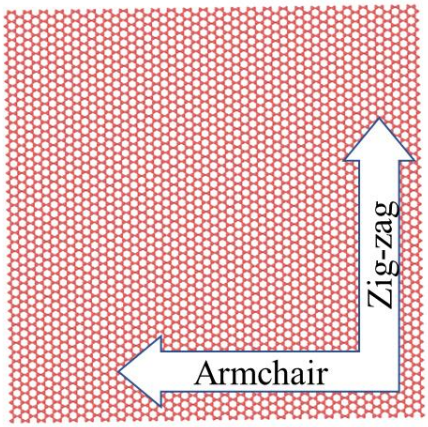

Figure 3.5 Single-layer graphene sheet.

Fig. 3.5 shows a single-layer graphene sheet of 109 Å × 109 Å. This structure was subjected to strain. In this sheet hexagonal graphene is arranged in a continuous way. With lattice constant of 1.4 Å

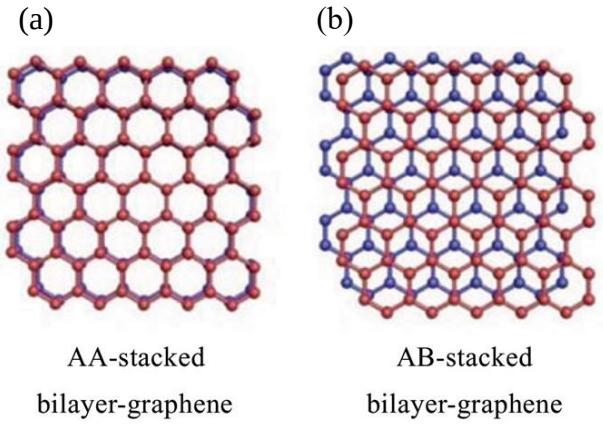

Figure 3.6 (a)AA Stacked and (b)AB stacked (Bernal) graphene.

A double layer graphene sheet of the same dimension was simulated in MD simulations. The interlayer distance of graphene was kept at 3.4 Å. The stacking of this bilayer graphene is AA stacking where all the carbon atom on the upper layer are overlapping the carbon atoms in the lower layer. While in the AB stacking, the carbon atom of the upper layer is in the center of the hexagon structure of the lower layer. Due to this structural arrangement, AB stacked graphene is very stable and exhibit exceptional optical and electrical properties[28].

Fig. 3.6 show the structure of AA stacked and AB stacked bilayer graphene. AB stacked (Bernal) graphene was also simulated to find its mechanical properties.

3.8.2 Water Confined Bilayer Graphene

This is an extension of bilayer graphene structures proposed in the previous chapter. The goal of this study is to analyze the effect of water molecules confined in nano-regions between graphene layers, on the mechanical properties and hydrophobic behavior of bilayer graphene. Bilayer graphene used in the previous study were filled with water molecules to study the effects of the quantity of water on its mechanical properties. The TIP4P 4 water model[62] is used in this simulation. The LJ potential discussed above was used with AIREBO to model the interaction between water molecules and graphene.

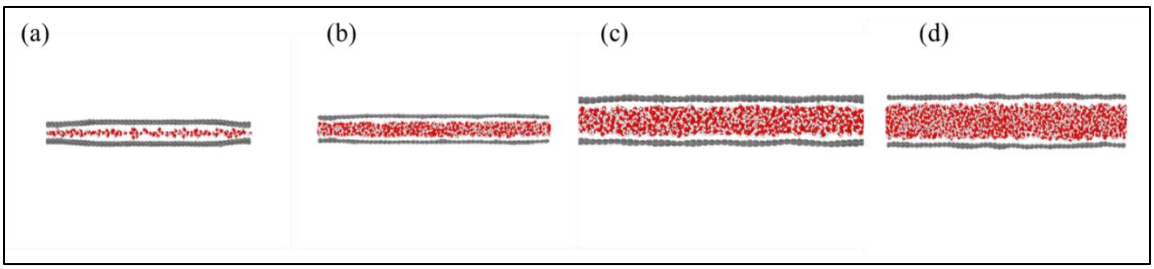

Figure 3.7 Bilayer graphene with different slit width

The interaction cut-off was set to be 1.92 Å for the carbon atoms. The LJ potential with globally accepted default parameter for potential energy cut-off and dielectric constant was used[63]. The slit width (distance between two graphene sheets in the z-direction) was varied along with the water content to analyze the effects.

Table 3.1 Slit Distances And % Of Water Mass of Water Confined Graphene

Type	% Water Mass	Slit width (Å)	No. of Water molecule
(a)	7.66	4.5	320
(b)	22	7.0044	960
(c)	33	9.5044	2160
(d)	46	12.044	2940

Table 3.1 shows the type of graphene with its slit width and percentage of water mass present in the structures shown in Fig. 3.7. All these structures were relaxed for 50 ns using the conjugate gradient (cg) method in LAMMPS during the pre-MD run. NVE ensemble with Berendsen thermostat was used to keep the temperature at room temperature (300 K). After the relaxation, a constant strain rate of 0.01 fs^{-1} was applied to study the behavior of water confined bilayer graphene and its mechanical properties.

During MD simulation the density of water molecule during relaxation and strain was recorded as a function of height using LAMMPS. The simulation box was divided into small bins having z-height of 2 Å. The densities of these bins were dumped at a fixed interval of time. The center of mass is also computed using LAMMPS.

CHAPTER 4

RESULTS AND DISCUSSION

A great degree of work has been previously done on graphene in order to investigate its mechanical[12], electrical[64] and thermal[42] properties. There are plethora of studies related to graphene and its derivative structures that investigate their intrinsic stress properties[65-67]. All these studies report graphene to be an exceptional 2D material with potential applications in all fields of science and technology. However, industrial applications of graphene fall short due to the unstable nature of free-standing single-layer graphene. Therefore, in order to avail advantages of strength and stability of graphene for any technology, graphene is utilized in the form of its structural derivatives such as bi-layer graphene. While bi-layer graphene is easier to synthesize and has mechanical properties assumingly very similar to that of single-layer graphene, effect of interlayer shear of its stability is often neglected. In this study, we have investigated the mechanical properties of bilayer graphene in detail by Molecular Dynamics (MD) simulation using LAMMPS software as described in the methodology section. The results of the simulations and the observations are presented in this chapter.

4.1 Single and Bilayer Graphene under mode I tension

Ever since its discovery in 2004[5], Graphene has been called out for being one of the strongest materials out there. However, for several practical applications, graphene is usually employed in the form of bi-layered structure as single-layer graphene is very

difficult to isolate. In this section, the mechanical strength of the single-layer and bi-layer graphene is analyzed and compared in order to establish base results for further analysis.

A single-layer graphene sheet was subjected to strain in armchair and zig-zag direction at the strain rate of 0.001 fs^{-1} to investigate its elastic behavior and mechanical properties. Fig.4.1 shows the behavior of graphene under uniaxial strain in a zig-zag as well as armchair direction. As we can see the stress limit in zig-zag direction is much higher than in armchair direction. The intrinsic stress of zig-zag graphene is $\sigma_{zig\text{-}zag}$ = 136.71 GPa and the strain is $\varepsilon_{zig\text{-}zag}$ = 0.259. And the intrinsic stress and the strain is $\sigma_{armchair}$ = 102.8 GPa and $\varepsilon_{armchair}$ = 0.17,respectively. These results are in concordance with experimental reports[12].

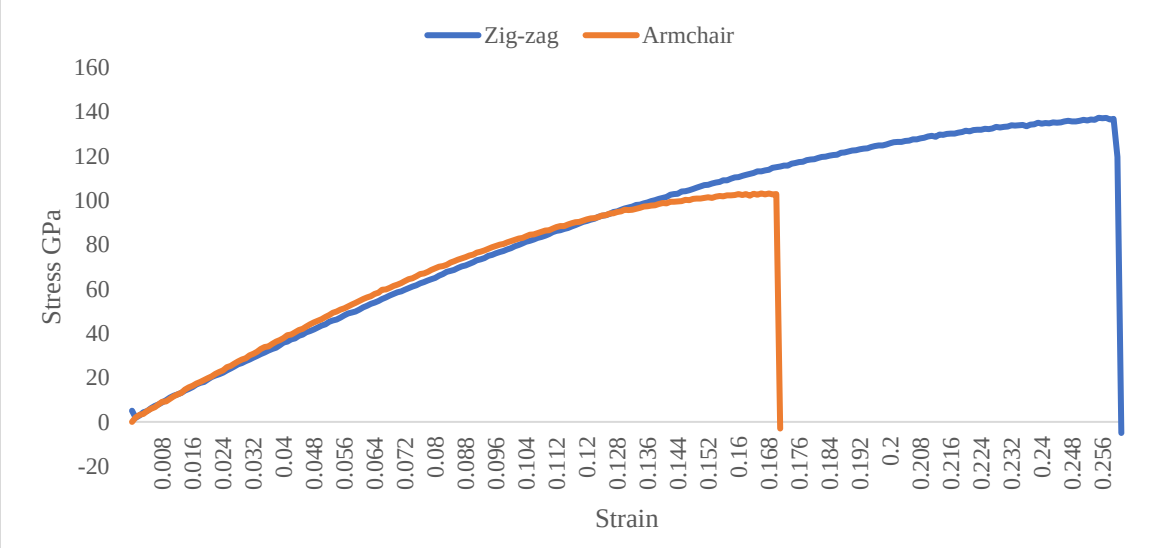

Figure 4.1 Stress versus Strain of single-layer graphene under uniaxial pull in zig-zag and armchair direction.

These results show that a graphene sheet under uniaxial mode I tension exhibits higher tensile strength in the zig-zag direction. This further confirms that AIREBO potential is a preferable option when it comes to molecular simulation of graphene under tension. Some previous similar studies of MD employed with AIREBO potential have also shown identical values as theoretical results based on Griffith's criterion[57].

Fig. 4.2 shows the behavior of bilayer graphene under uniaxial strain in Zig-zag as well as armchair direction. As we can see the stress limit in zig-zag direction is much higher than in armchair direction. The intrinsic stress of zig-zag graphene is $\sigma_{zig\text{-}zag}$ = 84.04 GPa and the strain is $\varepsilon_{zig\text{-}zag}$ = 0.251. And the intrinsic stress and the strain is $\sigma_{armchair}$ = 64.85 GPa and $\varepsilon_{armchair}$ = 0.171, respectively. One interesting observation was that during uniaxial

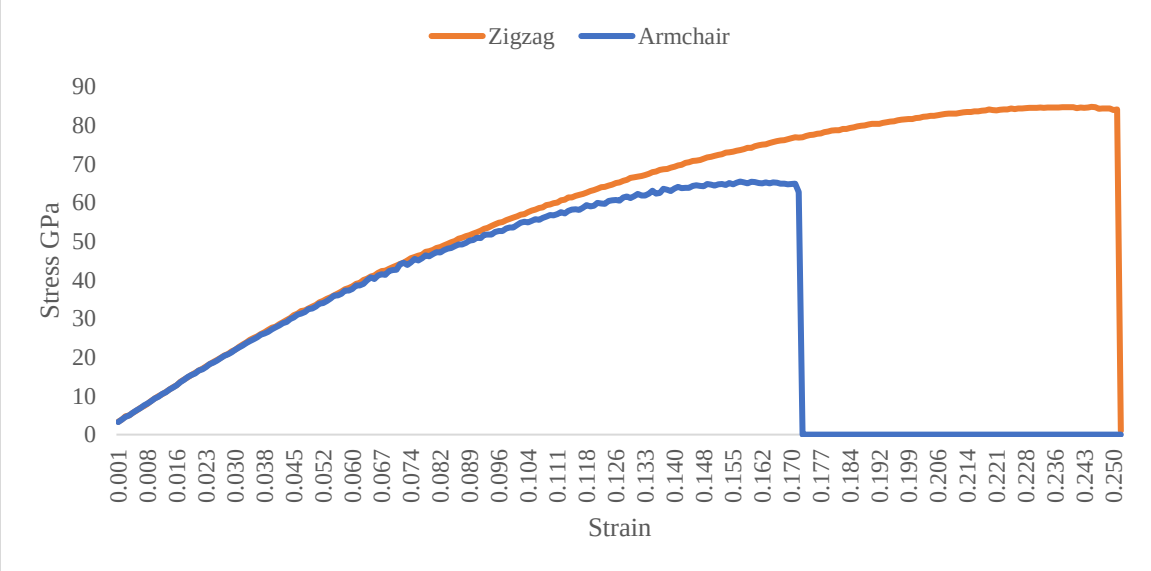

Figure 4.2 Stress versus Strain of bilayer graphene under uniaxial pull in zig-zag and armchair direction.

loading, It was concluded that bilayer graphene does not exhibit as strong stress limit as a single graphene sheet possibility due to shear between the two layers. These results are in line with previous reports in the literature and validated out simulation model for further analysis[29].

4.2 Crack Propagation in Single and Bilayer Graphene

Once it was established that bi-layer graphene falls short in terms of stress limit as compared to single-layer graphene, we intended to further emphasize the potential role of a substrate graphene layer on the crack propagation phenomenon in the top layer. In order to investigate the crack propagation phenomena, single and bilayer graphene sheets of 36×36 nm were strained under a strain rate of 0.01 fs^{-1}. Single-layer graphene and a top layer of the bi-layered structure has a crack of 10 Å at the center in an armchair direction the position of the crack can be seen figure 4.5. The size of the graphene layer was taken at least 10 times the crack length in order to avoid the effects on finiteness.[68]

The strain was applied in the zig-zag direction. The results were noted every 0.1 ps during simulation to analyze the crack propagation with time. The aim of this simulation was to also find out the impact of a van der Waal effects from the substrate lattice on the crack propagation phenomena of the top graphene layer. Fig. 4.3 shows the initialization of crack propagation in single and bilayer graphene. The time step at which the crack propagation initializes in both the case varied greatly. In the case of bilayer graphene, it starts at 220.4ns and in the case of single-layer, it starts at 221.8ns. The results for single-layer graphene are similar to the previously published reports[28]. Notably, the stress-strain

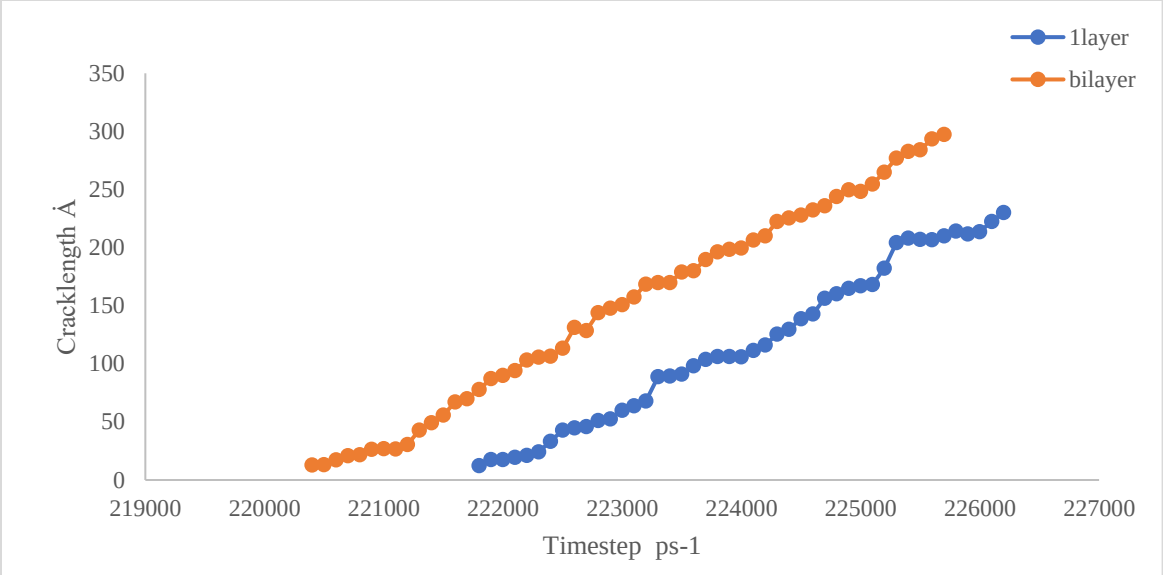

Figure 4.3 Initialization of propagation of crack with timesteps in single and bilayer graphene.

values of cracked graphene are low compared to the results of pristine graphene in section 4.1. The intrinsic stress and strain for single-layer with crack is σ = 93.24 GPA and ε = 0.123, and for the bilayer it is σ = 54.69 GPa and ε = 0.12 only. Which is predictable due to the higher strain rate applied. It is evident that the cracked bilayer graphene is weaker than the single-layer cracked graphene very similar to the results of the previous section.

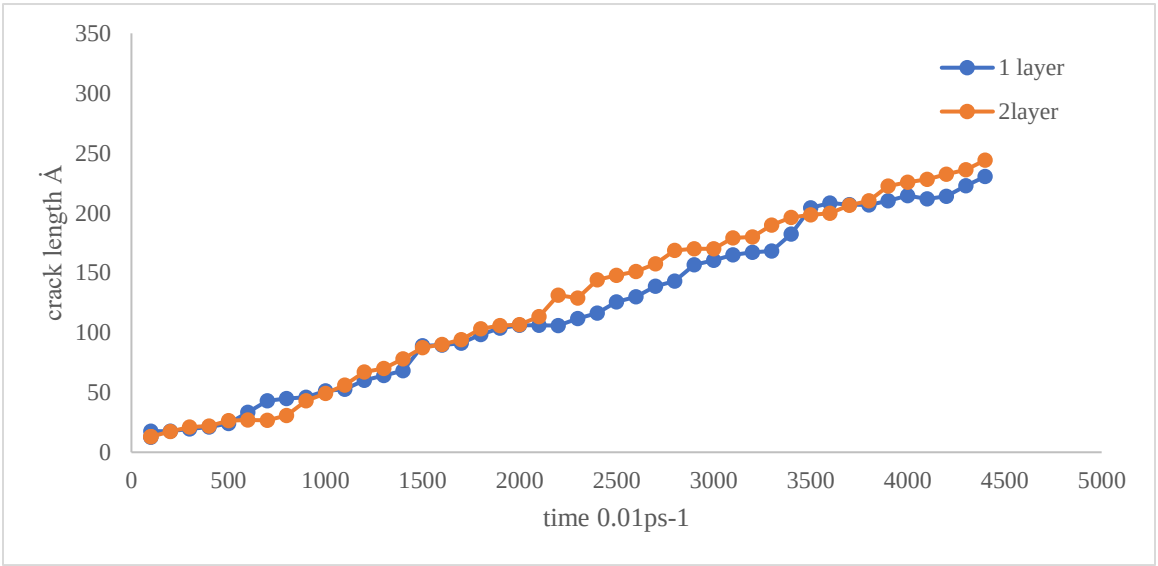

Figure 4.4 Propagation of crack with time in single and bilayer graphene

Fig. 4.4 shows the rate of crack propagation with time after initialization. Although the crack propagation started early in bilayer graphene, it was observed that after the initiation of crack propagation, the rate at which the crack propagates is not affected by the presence of substrate lattice.

Fig. 4.5 shows snapshots of simulation during crack propagation in a single-layer graphene sheet. It can be seen that the maximum stress value is at the edge of the crack. And the crack is propagating in only one direction that is perpendicular to the direction of loading (zig-zag) direction.

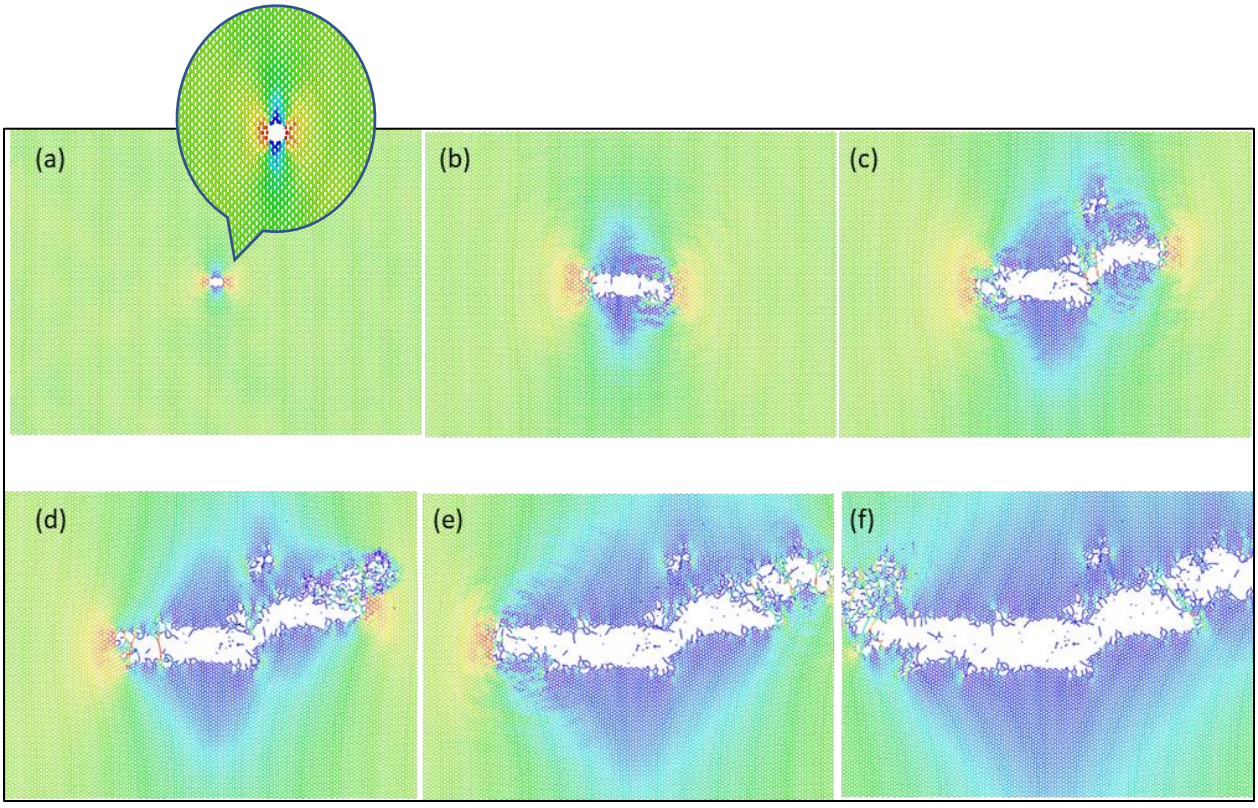

Figure 4.5 Crack propagation in single-layer graphene at different time step.

Fig. 4.6 shows snapshots of crack propagation simulation in bilayer graphene. It can be seen that the upper and lower layer during the strain at the same time. The the

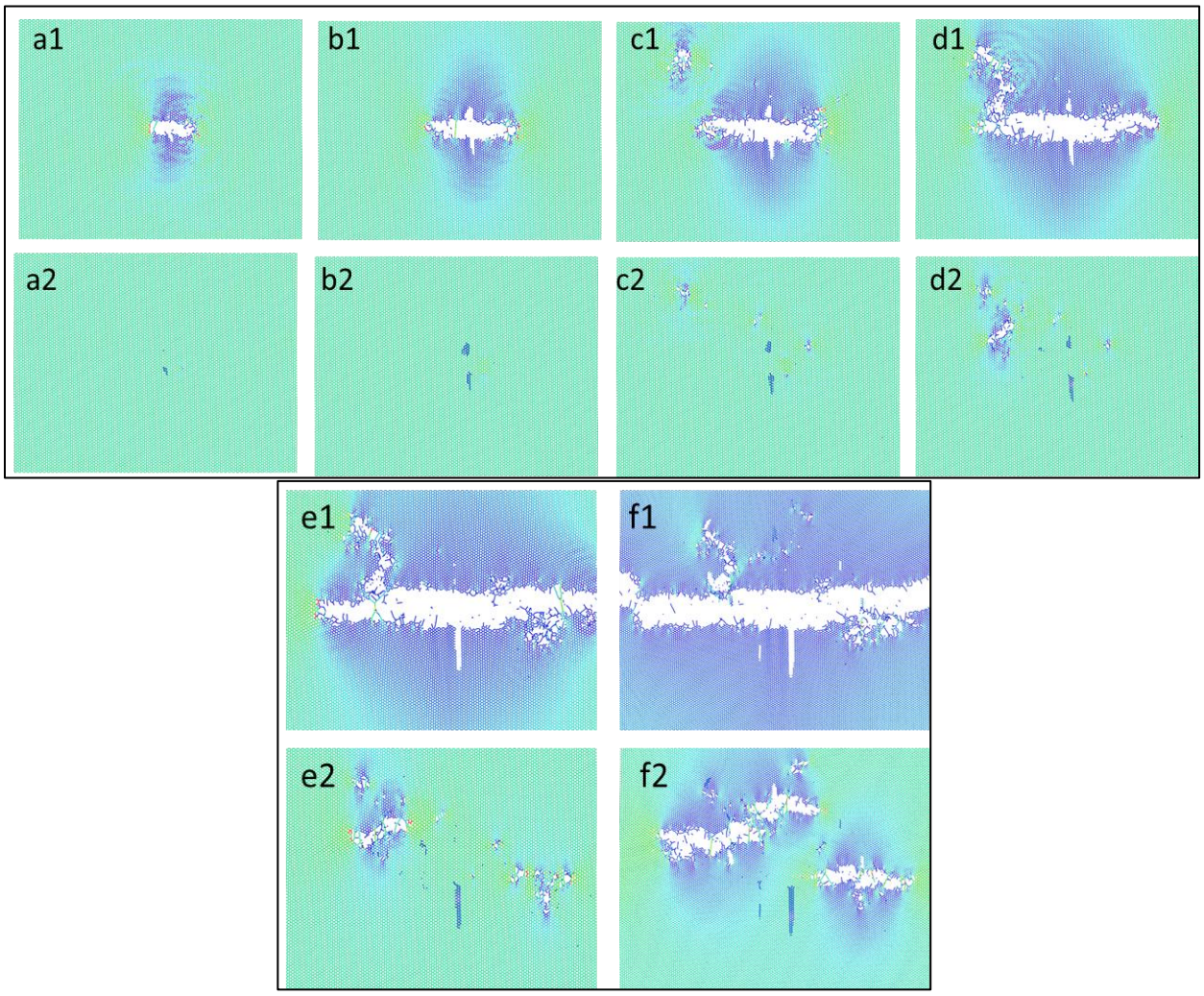

Figure 4.6 Crack propagation in bilayer graphene with 10 Å on upper layer at center of sheet in perpendicular direction to tensile load.

fig. 4.6 **(a1:f1)** shows the upper layer and fig. 4.6 **(a2:f2)** shows the lower layer during different timesteps of the simulation. It is interesting to observe the way crack propagated in the armchair as well as in the zig-zag direction (as shown in snapshot b1 and d1). While the upper layer is having very high-stress concentration, the lower layer is still intact until

the crack in upper layer starts to propagate in the zig-zag direction. It can be seen in d2 that as the crack in the upper layer propagated out of the crack plane the stresses in the lower layer also goes up as it starts cracking. It is visible in a2,b2 and c2 the stress in the region on the lower layer is going up. Also in the f2 snapshot, it can be seen the lower layer graphene starts fracturing only after the upper layer has completely collapsed.

4.3 Strain Intensity Factor in Graphene

The stress intensity factor **K** is used in fracture mechanics to predict the stress state ("stress intensity") near the tip of a crack or notch caused by a remote load or residual stresses. The graphene that was stained under mode I tension to check its elastic properties, similar graphene sheets were put under tension in the presence of 10Å crack in the armchair direction as shown in Fig. 4.5. The strain was again applied in a zig-zag direction. In this section, the main purpose is to find the stress intensity factor (SIF) of these graphene sheets and compare the results of single, bilayer graphene and Bernal graphene. It is crucial to

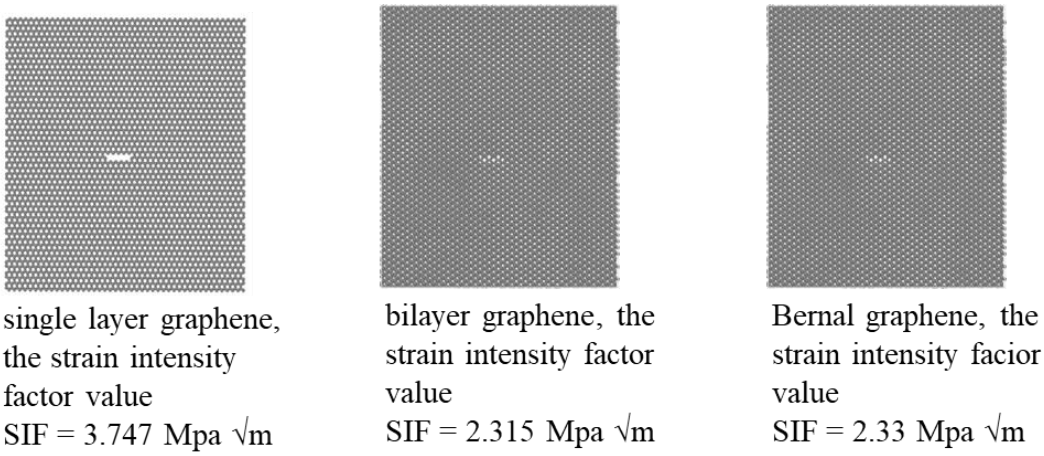

Figure 4.7 Stress intensity factor in single, bilayer and bernal graphene. In zig-zag direction.

verify if the turbostratic orientation of stacked layers affected the crack propagation phenomenon somehow.

Fig. 4.7 shows the stress intensity factor calculated according to Eq. 3.10. For 1-layer pristine graphene, SIF was calculated to be 3.747 Mpa √m. While AA stacked graphene and AB stacked graphene exhibit lower SIF values as the structure itself is weaker than single pristine graphene as observed in the previous sections 4.1 and 4.2. For single-layer pristine graphene, our results matched with the previously reported works. AA stacked graphene and AB stacked graphene is it still a subject of study.

4.4 Elastic Properties of Turbostratic Bilayer Graphene

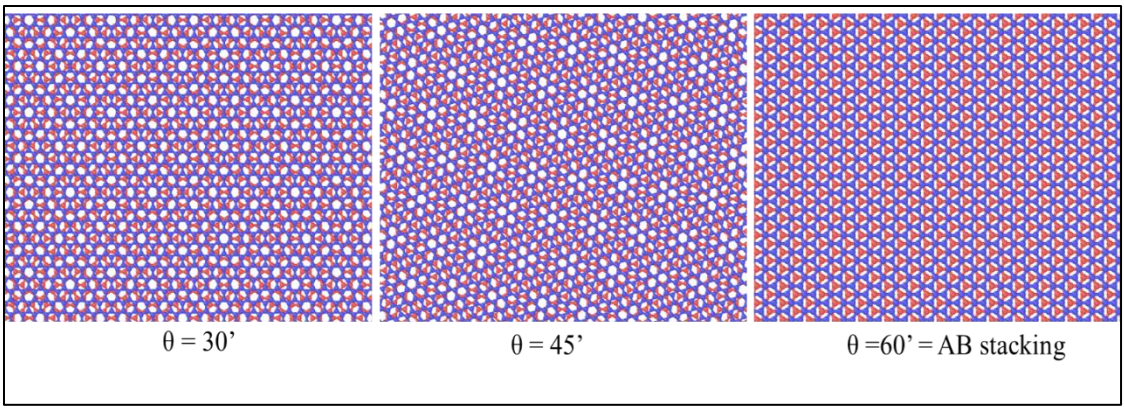

Figure 4.8 Bilayer graphene with different crystallographic angle (θ).

Recent studies have shown that turbostratic bilayer graphene with different crystallographic angle shows exceptional electronic and optical properties. Thus, having a wide range of application than single-layer graphene. However, mechanical properties of such differently oriented bi-layers are still mattered of investigation for researchers. In this

chapter mechanical properties of turbostratic bilayer graphene with different crystallographic angle has been studied.

Fig. 4.8 shows the structures of turbostratic bilayer graphene with different crystallographic angles. In order to compare it with normal bilayer, the dimensions of graphene sheets were kept the same. Fig. 4.9 shows the final energy state of all the structures after the relaxation of 50 ns. As we can see graphene with the crystallographic angle of 60′ is the most stable among all graphene variations. Coincidently it is the same structure as AB(Bernal) stacking[26]. Post relaxation, all turbostratic bilayer graphene variations were stressed at a constant strain rate of 0.01 fs^{-1}. Results of these simulations are shown in Fig. 4.9

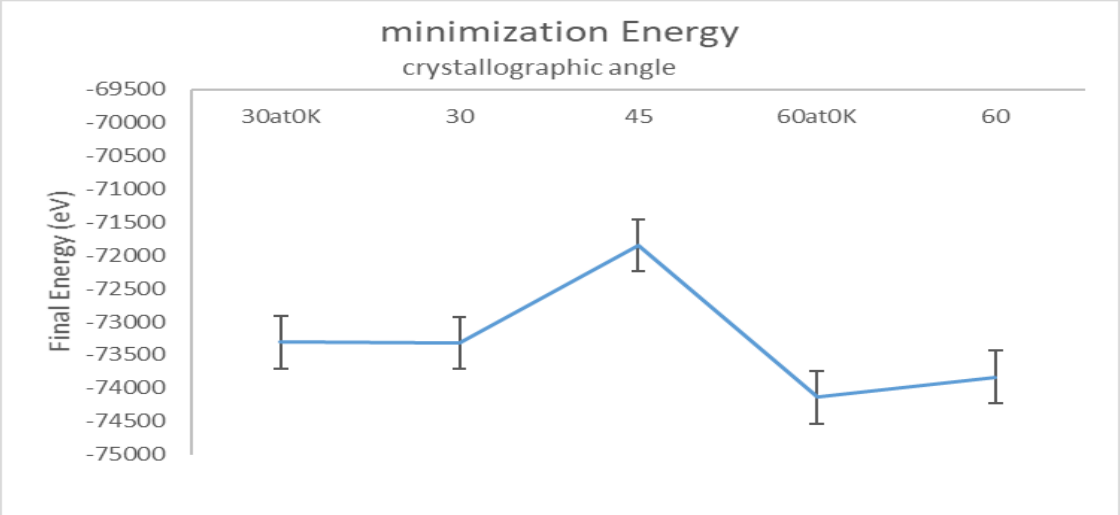

Figure 4.9 Minimization energies of different with different crystallographic angle.

Fig. 4.10 shows the stress versus strain results of turbostratic bilayer graphene. From these results, it was observed that AA stacked, and AB stacked (Bernal) graphene are more stable than the other turbostratic bilayer graphene structures. Their energies after relaxation are much higher than pristine graphene of the same size. Their behavior under strain was also quite different then AA stacked, or AB stacked (Bernal)graphene.

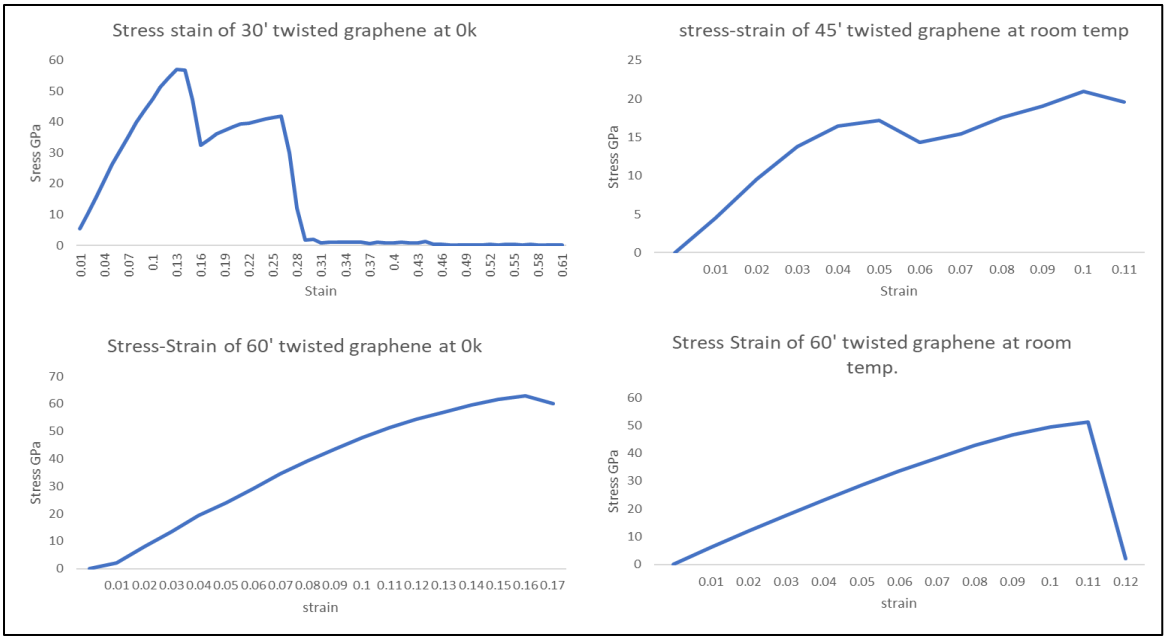

Figure 4.10 Stress - strain curves obtain by MD simulation of turbostratic bilayer graphene with crystallographic angle of (a) 30', (b) 45', (c) 60' at 0K and room temperature.

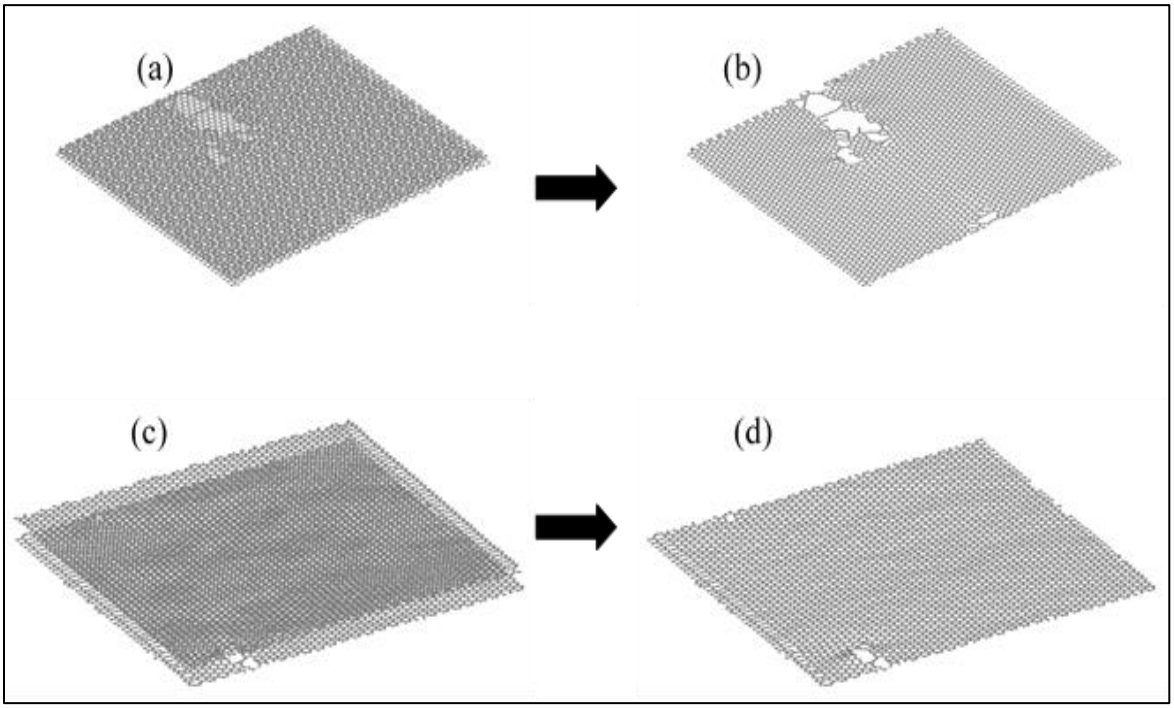

Figure 4.11 Snapshots of turbostratic bilayer graphene during strain at a point where fracture initialize. (a) turbostratic bilayer graphene with crystallographic angle of 30' at 0K. (b) sliced graphene showing only lower layer of image in the left where crack initiate. (c) turbostratic bilayer graphene with crystallographic angle of 60' at 0K. (d) sliced graphene showing only lower layer of the left image where crack initiate.

Pristine graphene has a linear stress-strain curve as seen in chapter 4.1 and 4.2 while turbostratic graphene with the crystallographic angle of 30 and 45 do not exhibit the same behavior.

Their stress stain curve has two peak stress values instead of one. Fig. 4.10 shows the snapshots of graphene at a crystallographic angle of 30 and 60 at 0K temperature. It was observed that in both the case the crack is appearing first in the lower layer of graphene. That means that the lower layer is under higher stress than the upper layer. These results show the same pattern as chapter 4.1 but were not in accordance with the results shown in chapter 4.2 wherein the presence of a crack, the stress was transformed to a lower layer at the last stage.

Based on these results, it can be concluded that in bilayer graphene the fracture tends to start in lower layer first if there is a crack present in the upper layer then the results can be same as shown in chapter 4.2. that if a crack is present in the upper layer, the lower will start to fracture under strain when the upper layer is totally fractured.

Table 4.1 shows a comparison between all the graphene structure that were tested in this study. It shows the minimization energy after relaxation, stress limits and strain limits in armchair direction. It was observed that among all the graphene structures, pristine bilayer graphene is the least stable but strong structure with stress limit of 65.3 GPa. And single-layer pristine graphene is the strongest structure among all the variations with stress limit of 102.8 GPa.

Table 4.1 Minimization Energy, The Tensile Stress in Armchair Direction, And Strain Limits Of Single, Bilayer, Bernal And Turbostratic Bilayer Graphene

Graphene type	minimization energies(eV)	tensile strength (GPa)	tensile strain
single-layer graphene	-35132.2581	102.8	0.17
bilayer graphene	-35020.7	65.3	0.171
Bernal graphene	-72852.63007	64.7	0.169
30' at 0K	-73310.37446	57.1	0.13
30' room temp.	-73322.28075	64	0.16
45' room temp.	-71852.40786	21.19	0.11
60' at 0K	-74139.71592	62.86	0.17
60' at room temp.	-73832.09889	51.74	0.12

4.5 MD Simulations of Water Confined Graphene

The exceptional mechanical properties of graphene and its bilayered derivatives are discussed until now. However, graphene used in various application as discussed in the introduction is often exposed to water or vapors in the form of humidity. Water-Graphene interaction is an obligatory possibility to investigate. Multiple studies show water behavior when confined to CNT or graphene [35, 69]. In this chapter, the study of mechanical properties of graphene in the presence of variable water molecule and effects of slit width have extended where slit width is the distance between two graphene sheets. And the behavior of water confined in graphene is also further analyzed.

In order to check the mechanical properties of the water confined graphene. Different structures were minimized, and MD was run for 50 ns. It was observed that with

variation in slit width stability of water confined graphene can be optimized according to its application.

Fig. 4.12 shows water confined bilayer graphene with different slit width. These structures were relaxed to perform the further simulation. The final energy of these structure after relaxation is presented in a table with the value of its slit width.

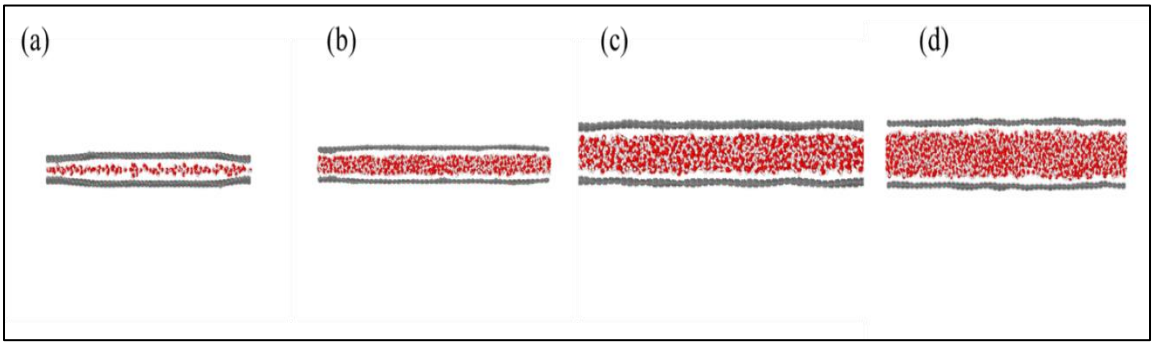

Figure 4.12 Water confined graphene with different slit width.

Table 4.2 Minimization Energies Slit Width and No, Of Molecules Of Water In Water Confined Graphene

Type	Slit width (Å)	No. of Water Molecules	Minimization energy(eV)
(a)	4.5	320	-46815.59
(b)	7.0044	960	-47110.46
(c)	9.5044	2160	-72645.33
(d)	12.044	2940	-72908.17

From the data shown in table 4.2, it can be observed that as we increase the slit width the final energies are decreasing. So, if the distance between two graphene sheets is higher and water molecules have more free space to move. As a result, it leads to a more

stable structure. In this case, the graphene with a slit width of 12.044 Å is the most stable structure with the final energy of -72908.17 eV.

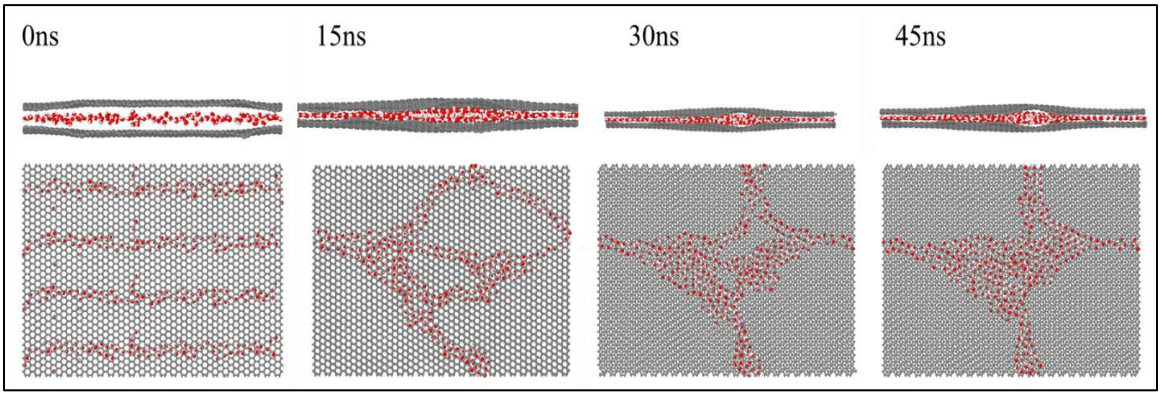

Figure 4.13 Water confined bilayer graphene with slit width 4.5Å at different time step during relaxation.

Fig 4.13 Shows the water confined bilayer graphene with a slit width of 4.5 Å during minimization at a time interval of every 15 ns. At 0 ns the graphene is at normal state and the water has started moving between bilayer. After 15 ns water molecule has

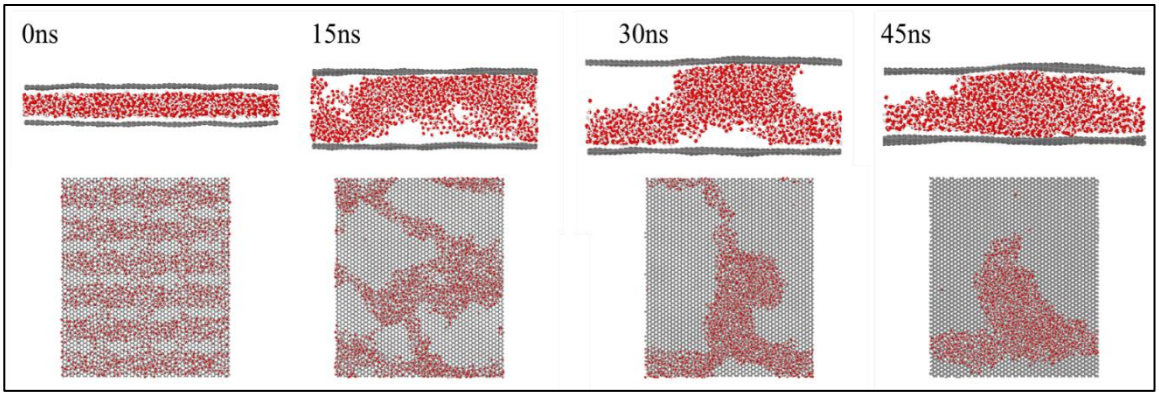

Figure 4.14 Water confined bilayer graphene with slit width 9.5044 Å at different time step during relaxation.

formed a capillary according to its adhesive forces and presence of the weak hydrogen bonds[70]. By this point, the graphene sheet has started to cover the water molecules. At 30 ns, water density at the center of the graphene increases and the graphenes form a wrap-

like structure around the water molecules. This kind of inherent surface hydrophilic behavior is also reported in previous studies[48]. At about 45 ns of the simulations, water has its maximum density at the center of the graphene sheets with the slit width between the graphene at the corners decreasing to ~ 4.0 Å. However, at the center where the water has accumulated, the slit width is ~9.0 Å.

Fig. 4.14 shows the water confined bilayer graphene with a slit width of 9.5044 Å with the same time interval as the previous case. This case shows completely reverse the behavior of the graphene. As shown in fig 4.14, at 0 ns has a normal slit width (mention the value) and the water molecules have started moving in the system. But, after 15 ns the slit width has increased up to 30 Å and the water is again forming capillary due to adhesive forces. In this case, the size of the water channels is bigger due to the higher number of water molecules. After 30 ns, the graphene layers are still moving apart from each other for some more nanoseconds. When the graphene sheets have reached the maximum distance, the slit width started to decrease and stopped at ~22 Å with the water present between the sheets being concentrated around the center. The same behavior was also observed in the case of water confined graphene with a slit width of 12.044 Å. It also exhibited that the slit width increasing followed by a decrease after 35ns. In order to investigate the state of water during minimization, further the density and center of mass of water molecule were calculated.

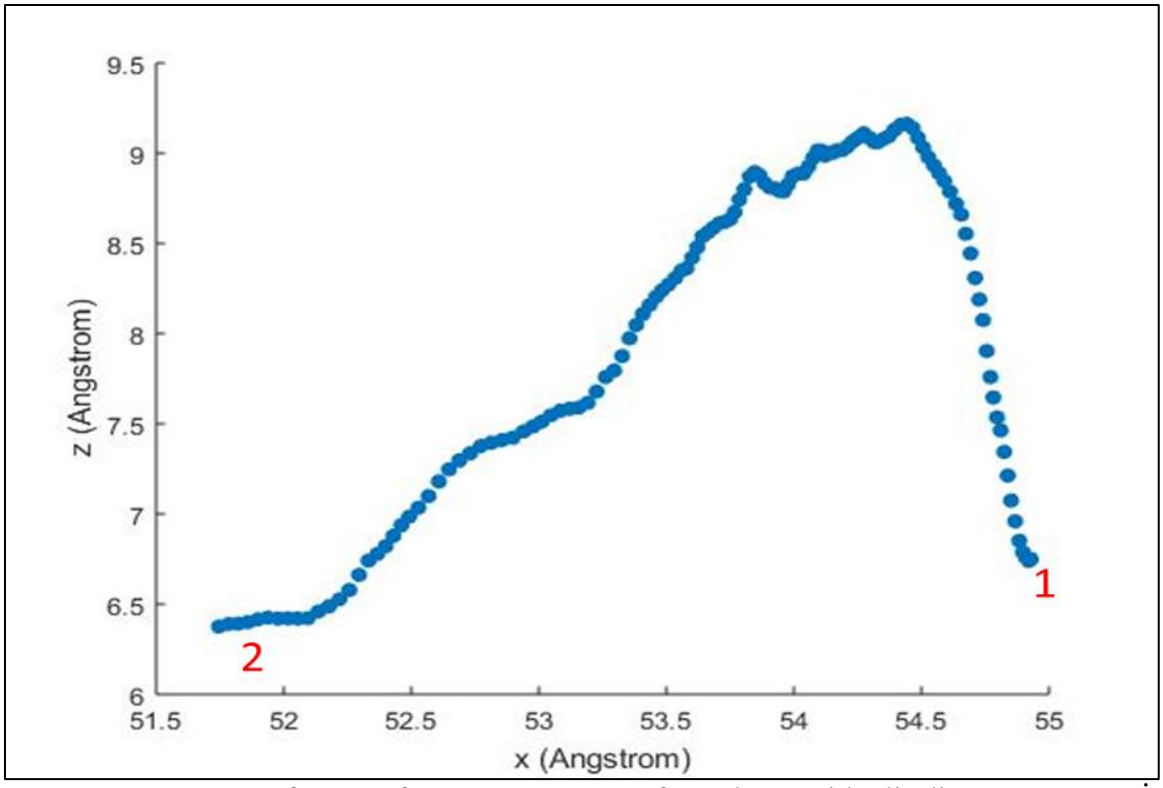

Figure 4.15 Center of mass of water molecules of graphene with slit distance 9.5044 Å moving in XZ plane during strain.

Fig. 4.15 shows the center of mass of water molecule moves in XZ-plane in water confine graphene with a slit width of 9.5044 Å. Point 1 is the start point of the curve and point 2 is the endpoint. This curve shows the movement of the center of mass for 50 ns throughout the relaxation process. During this process the center of mass of water molecule moves upwards in the z-direction and when the slit width is at its maximum its stats to come downwards. As can be seen in Fig. 4.14 where the slit width starts to reduce after a certain time. However, when the parameters were measured in water confined with a slit width of 12.044 Å and 2940 molecule slight change was observed.

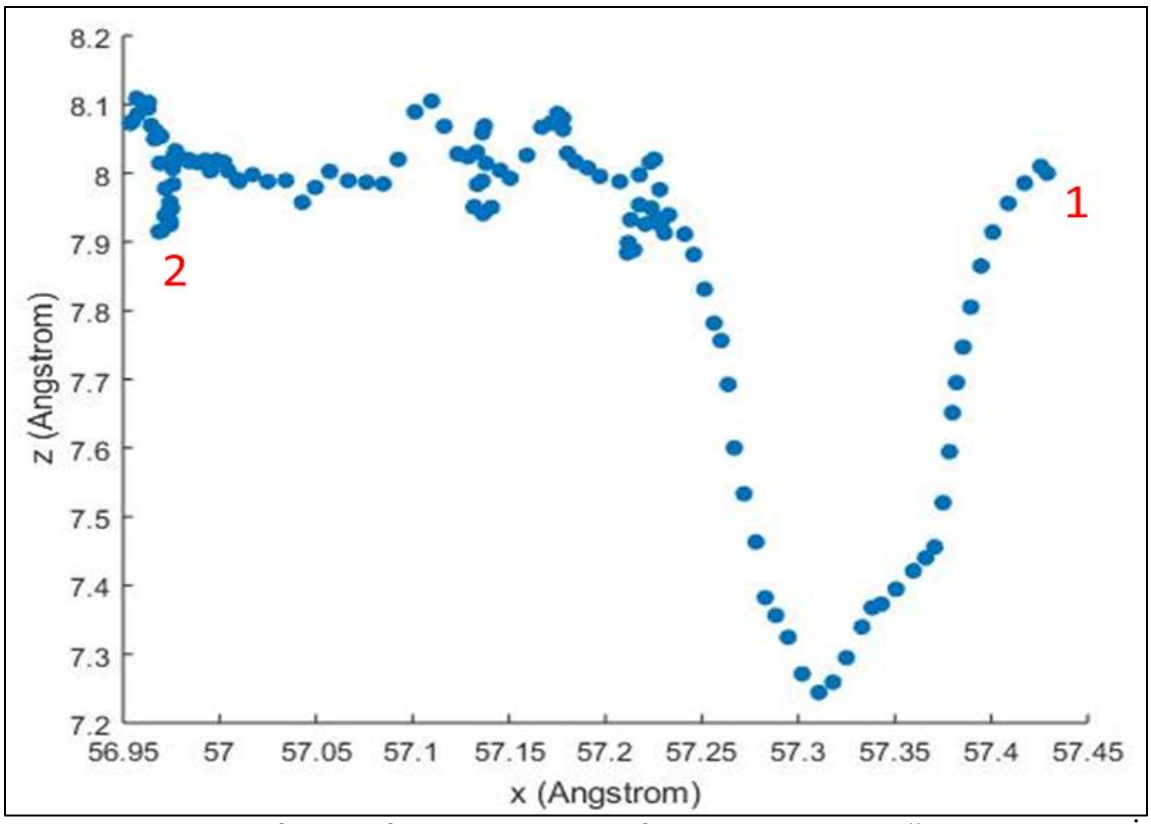

Figure 4.16 Center of mass of water molecules of graphene with slit distance 12.5044 Å moving in XZ plane during strain.

Fig. 4.16 shows the movement of the center of mass in XZ-plane of water confined graphene with a slit width of 12.044 Å. Unlike the curve in fig. 4.15 the center of mass did not move upward and then eventually came down. In this case, the center of mass starts is movement by moving downwards and then eventually moves back where it started. In this case, the movement in x-direction was almost none.

In order to further investigate the behavior of water confined in bilayer graphene, the density fluctuation between two graphene sheets was investigated. To get a clear picture of how water is distributed between two layers of graphene sheets density was measured bin wise where each bin's height was 2Å.

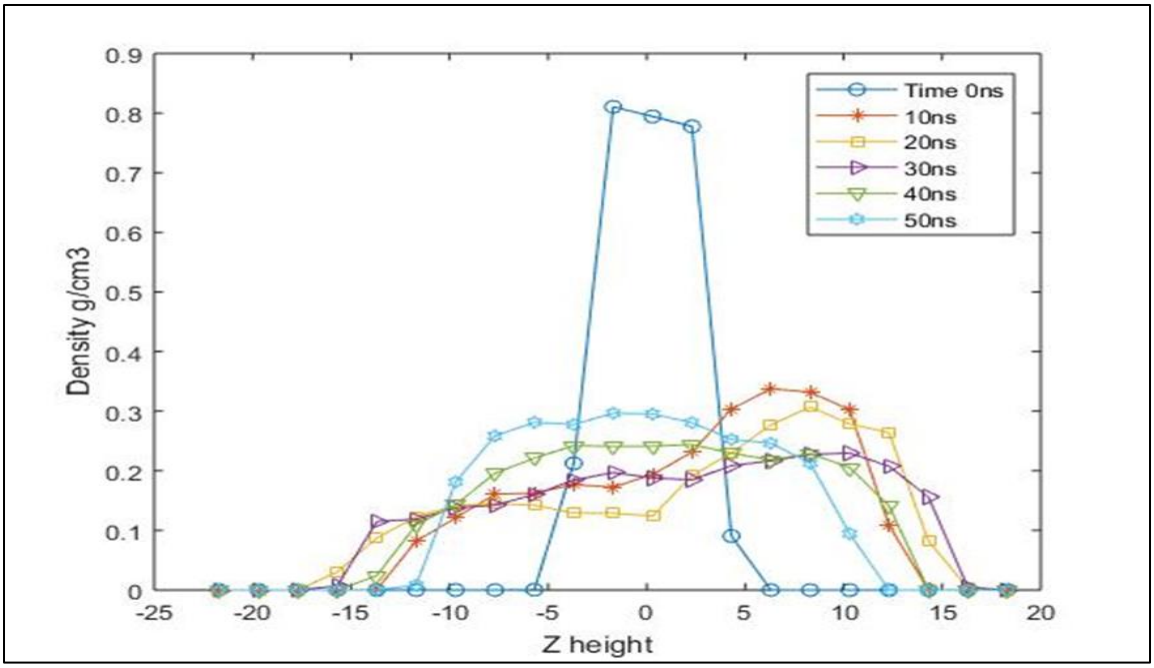

Figure 4.17 Density distribution of graphene with slit width 9.5044 Å changing with time during relaxation as a function of z dimension height.

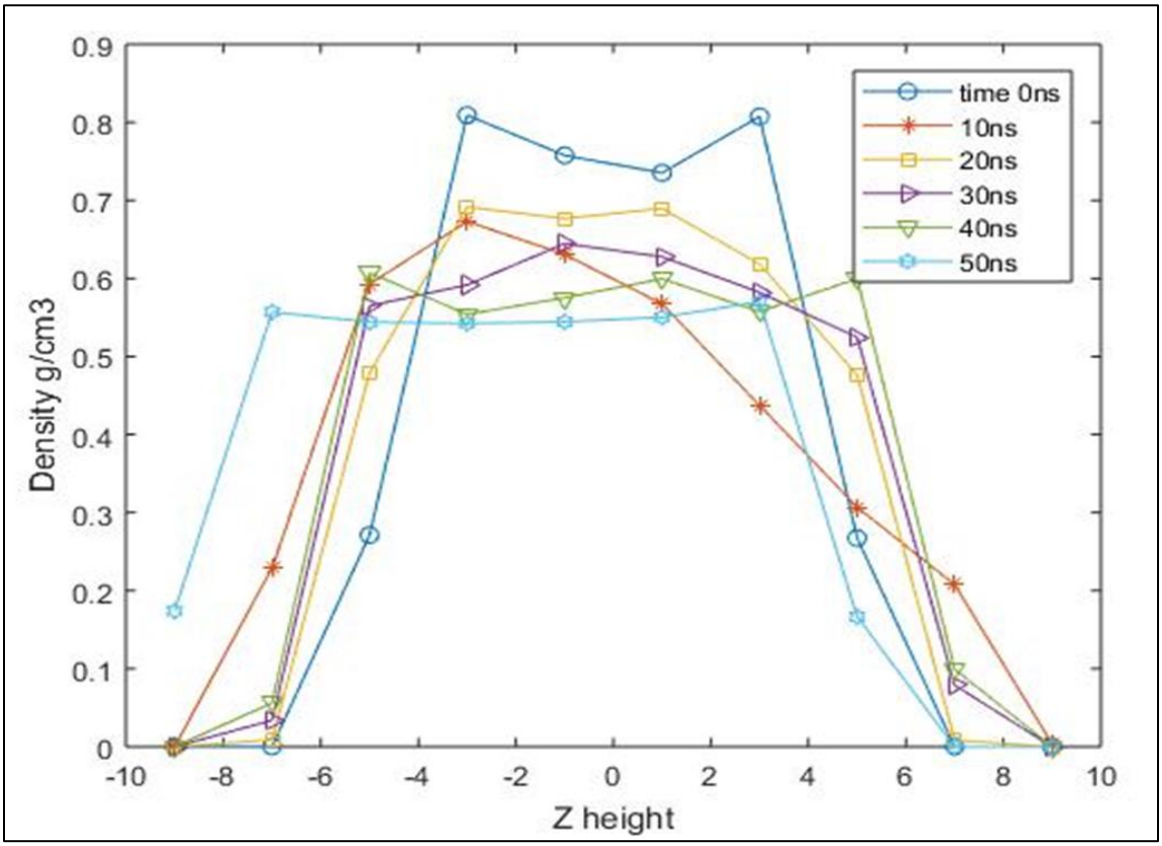

Figure 4.18 Density distribution of graphene with slit width 12.5044 Å changing with time during relaxation as a function of z dimension height.

Fig. 4.17 and fig. 4.18 shows density bun wise distribution of water molecule between graphene sheets. Here 0 on the x-axis is center between 2 graphene sheets and the x-axis is vertical distance (Å) while is y-axis is the density of water molecule(g/cm^3). During the relaxation of 50 ns, as the time goes the slit width is changing. And with that, the density distribution in the figure is changing. It was observed that as time passes the water tends to accumulate around the center of the graphene sheets. The density valuer at the center is at a peak at all measured time.

Results in this section showed some very interesting behavior of water confined graphene and movement of water molecules trapped by graphene sheets. As graphene is known to be hydrophobic when available in single-layer[38]. Although it is sometimes also hydrophilic based on how it was synthesized [71] or how it's stacked [72]. The results in fig. 4.13 showed that when the slit width is 4.5Å and number of molecules are very few against the size of graphene sheets, the graphene sheets try to encapsulate water due to van der Waals interaction with a water molecule. But when the slit width is large, and no. of the water molecule is relatively in large number graphene sheets tends to repeal each other during relaxation. Density distribution also shows that water also tends to collect center and not on the surface of graphene. From these results, it can be concluded that behavior water confined graphene sheets and water in it can also be related to the quantity of water molecule and the slit width.

4.6 Elastic Properties of Water Confined Graphene.

The behavior of water confined graphene during relaxation was discussed briefly in the previous chapter. That study has been extended in this chapter. The single-layer graphene possesses exceptional mechanical strength[12]. But how its elastic behavior changes in the presence of water is a still matter of grate interest among researchers. In this chapter, the behavior of water confined bilayer graphene under uniaxial stress has been investigated.

Same as chapter 4.1 all structure shown in Fig. 4.12 were subjected to uniaxial stress in zig-zag as well as armchair direction with the strain rate of 0.01 fs^{-1}. The periodic boundary conditions are applied to this simulation. All the minimized structure from chapter 4.5 were used in this simulation to check their elastic properties. The results and observation of the simulation are as follows.

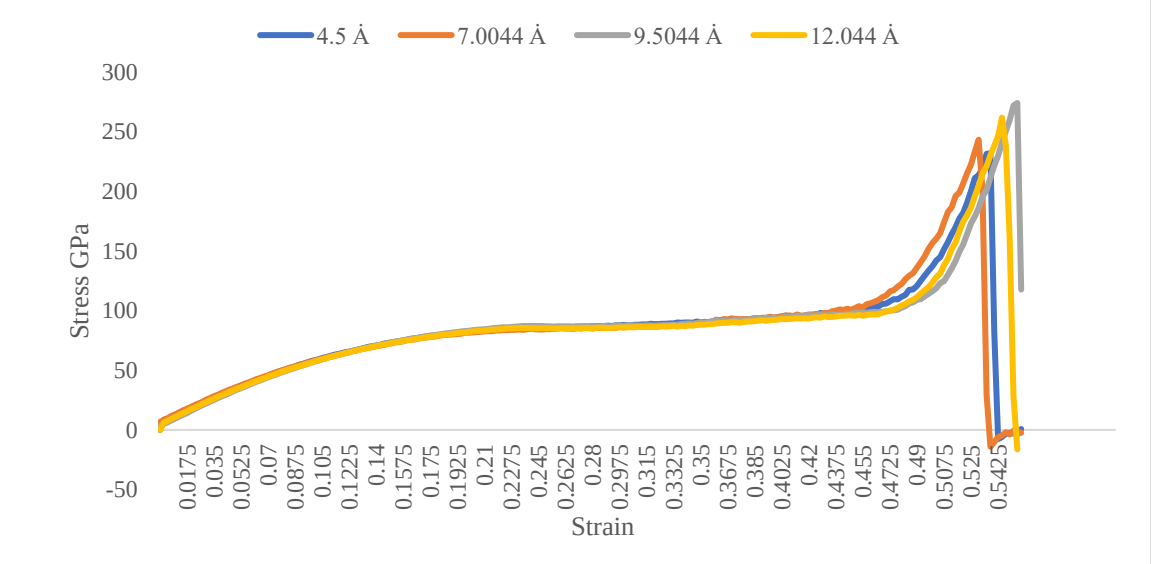

Figure 4.19 Stress versus strain comparison of water confined bilayer graphene with different slit width in zig-zag loading.

Fig. 4.19 shows the stress-strain curve of the water confined bilayer graphene with different slit width subjected to strain in a zig-zag direction. it was observed that in the presence of water molecule the elastic limits of bilayer graphene have incredibly increased. Normal bilayer graphene was cracked at 0.251 strain while the stress limit of water confined graphene is observed to go up to ≈ 0.5235. And the stress limit is ≈ 250 GPa.

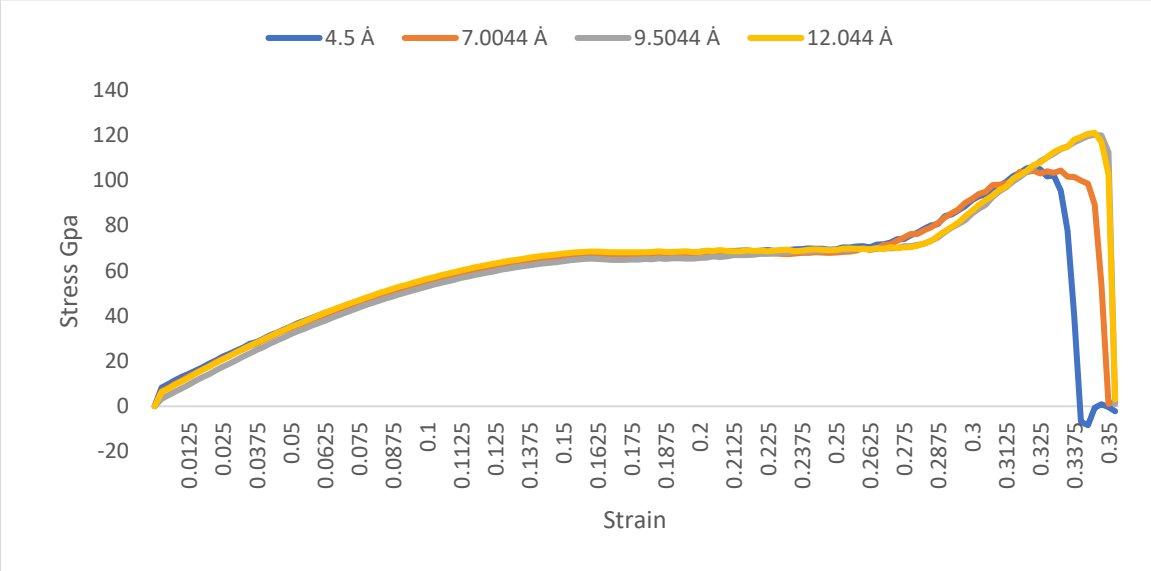

Figure 4.20 Stress versus strain comparison of water confined bilayer graphene with different slit width in zig-zag loading.

Fig. 4.20 shows the stress-strain curve of the water confined bilayer graphene with different slit width subjected to strain in an armchair direction. the strain limit in this simulation was ≈0.335 and the stress limit was observed ≈110 GPa. These values are significantly higher than normal bilayer graphene. It can be concluded that the presence of a water molecule is stopping the carbon bonds to break. This can be possible due to the adsorption of water molecules on the graphene sheet. Previous works have shown that the π electron present in graphene makes it very sensitive to humidity[73]. Further experiments

are required to confirm the theory. It was also observed that water confined bilayer graphene do not exhibit the same stress-strain curve as pristine bilayer graphene. Without water.

Table 4.3 Strain Stress Values for All Water Confined Graphene in Zig-Zag And Armchair Direction

slit width	Tensile stress (GPa)		tensile strain	
	zig-zag	armchair	zig-zag	armchair
4.5 Å	231	102.22	0.535	0.33
7.0044 Å	243	104.36	0.527	0.3325
9.5044 Å	274	120.14	0.555	0.345
12.044 Å	261	121.06	0.545	0.345

Table 4.3 shows the tensile stress and strain values of water confined bilayer graphene. It was observed it is more resistive to stress in zig-zag direction ten armchair direction. compare to pristine bilayer graphene its tensile strength was significantly higher

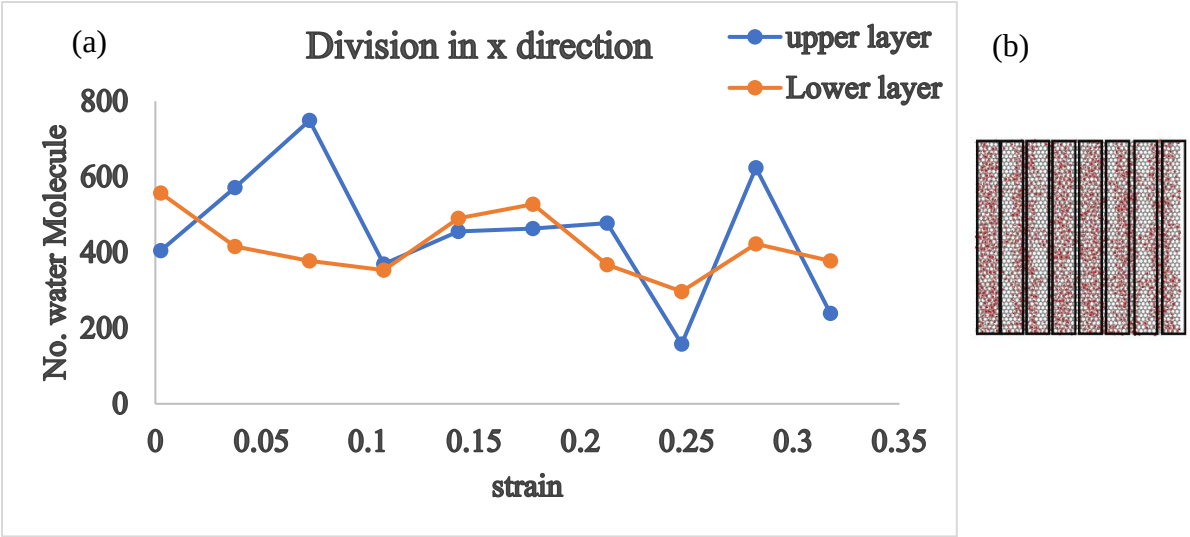

Figure 4.21 (a) Change in no. of water molecule present in the contact area of graphene sheets in water confined graphene with strain. (b) Bin vise division of the structure in X - direction.

in zig-zag direction while in the armchair direction the change was not very big. It was also observed the during strain there is sudden peak after the water confined bilayer graphene is strained above 80% of its strain limit.

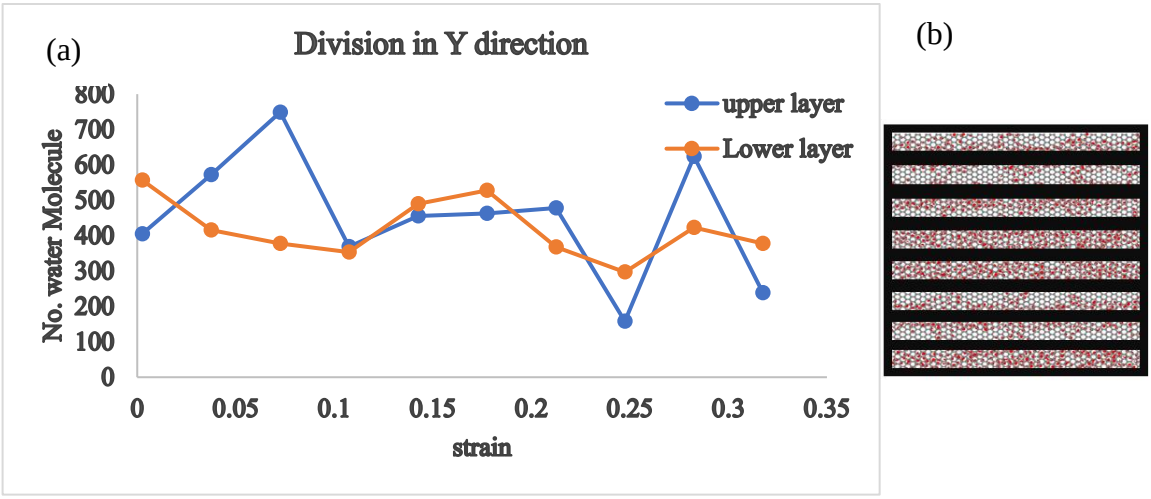

Figure 4.22 (a) Change in no. of water molecule present in the contact area of graphene sheets in water confined graphene with strain. (b) Bin vise division of the structure in Y - direction

In order to find the contact area of water and graphene sheets, some additional analysis was done. The surface contact area of water and graphene sheet was measured by[33]. According to the study water molecule present within 4 Å range of graphene, it is considered in the contact zone of graphene. Bilayer graphene was divided into bins of x-length × 5 Å × 4 Å and y-length × 5 Å × 4 Å as shown with the plot. The number of water molecules in this region was calculated and summed up to find the total number of water molecules in the contact zone. This measurement was taken as the structure is subjected to strain. The results are plotted in fig. 4.21 and fig. 4.22.

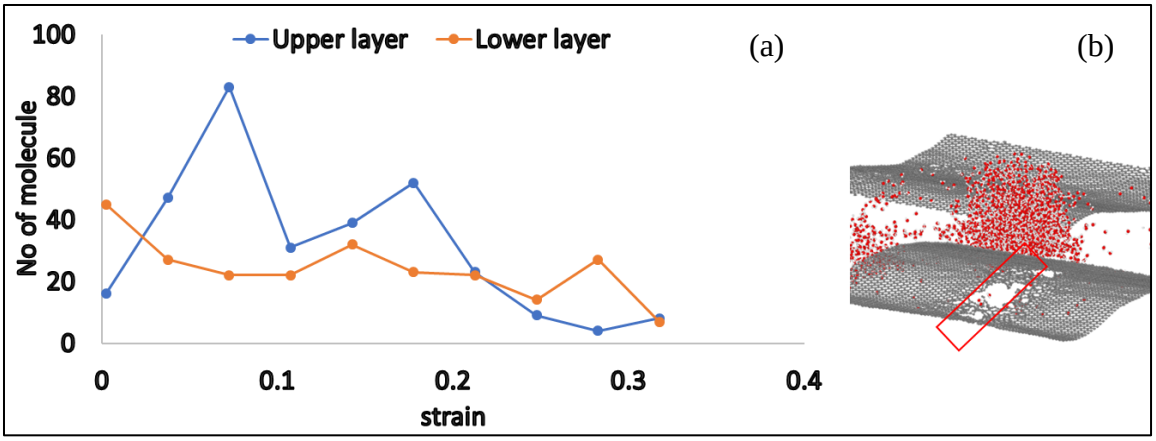

Figure 4.23 (a) Change in No. of water molecule with strain in the bin where the crack initiates. (b) the bin where the crack initiates.

Fig. 4.23 shows the number of the water molecule in the bin where the crack initiate during straining in armchair direction. it shows that by the time graphene fractured the

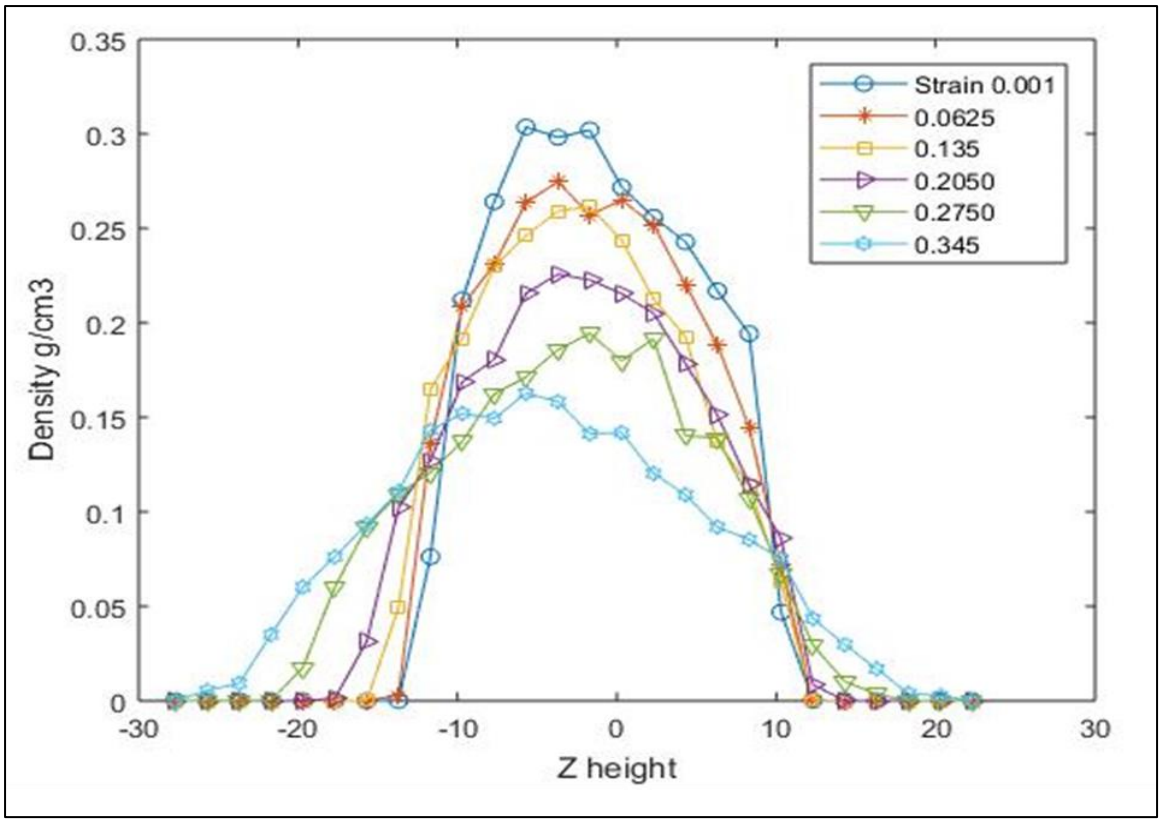

Figure 4.24 Density distribution of graphene with slit width 9.5044 Å changing with time during strain as a function of z dimension height.

no. of molecule in that area is minimum. The same behavior was observed in other cases.

Fig. 4.24 shows the density distribution of water molecule confined in bilayer graphene. Where 0 is the center of two sheets. The density distribution shows that water molecules are moving towards lower layer as strain increase. From the above results, it was observed that water molecule in the contact zone of the upper layer fluctuates more than in the lower layer. As the strain increase no. of water molecules in contact with both the layer has decreased. which shows the hydrophobicity of graphene. As he strain increase graphene sheets tends to move apart from each other. This behavior could be the results of hydrophobicity of graphene or some other force could be responsible for this. That is still a matter of further research.

CHAPTER 5

CONCLUSION AND FUTURE WORK

This work provides a study of mechanical properties of bilayer graphene with turbostratic orientations. MD simulations were used to find the tensile strength of single-layer graphene and the results were compared with previous work to verify the methodology. Post this, turbostratic oriented bilayer graphene structures were investigated. It was observed that AB stacked (Bernal) graphene is the most stable and strong graphene among other variations. Water confined bilayer graphene with different slit distance and water content was subjected to strain to observe the effects of water molecules on graphene structure. Water confined graphene was found to have significantly higher strain limit then bilayer graphene. A relationship between slit distance and tensile properties was also derived. With water content and slit length, graphene tends to change its hydrophobic behavior.

The result found in this study can be further extended by analyzing the relationship between water content and hydrophobicity. Additionally, the relationship between slit distance and hydrophobicity could also be investigated along with with the crack propagation in water confined graphene. Furthermore, the effects of other parameters like pressure and temperature on the motion of water molecule could throw more light on the applicability of bilayer graphene in sensor devices.

REFERENCES

1. Raju, A.P.A., et al., Wide-Area Strain Sensors based upon Graphene-Polymer Composite Coatings Probed by Raman Spectroscopy. Advanced Functional Materials, 2014. **24**(19): p. 2865-2874.
2. Papageorgiou, D.G., I.A. Kinloch, and R.J. Young, Mechanical properties of graphene and graphene-based nanocomposites. Progress in Materials Science, 2017. **90**: p. 75-127.
3. Cao, G., Atomistic Studies of Mechanical Properties of Graphene. Polymers, 2014. **6**(9): p. 2404-2432.
4. Mrmak, N. Graphene properties. 2014; Available from: www.graphene-battery.net.
5. Novoselov, K.S., et al., Electric Field Effect in Atomically Thin Carbon Films. Science, 2004. **306**(5696): p. 666-669.
6. Chowdhury, S. and R. Balasubramanian, Recent advances in the use of graphene-family nanoadsorbents for removal of toxic pollutants from wastewater. Advances in Colloid and Interface Science, 2014. **204**: p. 35-56.
7. Li, Z., I.A. Kinloch, and R.J. Young, The role of interlayer adhesion in graphene oxide upon its reinforcement of nanocomposites. Philosophical Transactions of the Royal Society A: Mathematical, Physical and Engineering Sciences, 2016. **374**(2071): p. 20150283.
8. Yang, X., H. Tian, and B. Zhang, Fast crack propagation correlated with crack tip stress in 2D hexagonal atomic lattices. International Journal of Fracture, 2018. **210**(1): p. 17-27.
9. Kim, K.S., et al., Large-scale pattern growth of graphene films for stretchable transparent electrodes. Nature, 2009. **457**: p. 706.
10. Geim, A.K. and K.S. Novoselov, The rise of graphene. Nature Materials, 2007. **6**: p. 183.
11. Novoselov, K.S., et al., Two-dimensional atomic crystals. Proceedings of the National Academy of Sciences of the United States of America, 2005. **102**(30): p. 10451-10453.
12. Lee, C., et al., Measurement of the elastic properties and intrinsic strength of monolayer graphene. Science, 2008. **321**(5887): p. 385-8.
13. Zhang, P., et al., Fracture toughness of graphene. Nature Communications, 2014. **5**: p. 3782.
14. Min, K. and N.R. Aluru, Mechanical properties of graphene under shear deformation. Applied Physics Letters, 2011. **98**(1): p. 013113.
15. Dewapriya, M.A.N., A. Srikantha Phani, and R.K.N.D. Rajapakse, Influence of temperature and free edges on the mechanical properties of graphene. Modelling and Simulation in Materials Science and Engineering, 2013. **21**(6): p. 065017.
16. Tsai, J.-L. and M.-J. Sie, Characterizing the Stress Intensity Factor of Graphene Sheet with Central Crack. Journal of Nanoscience and Nanotechnology, 2015. **15**(5): p. 3764-3772.
17. Xu, M., et al., A coupled quantum/continuum mechanics study of graphene fracture. International Journal of Fracture, 2012. **173**(2): p. 163-173.

18. Datta, D., et al., Effect of crack length and orientation on the mixed-mode fracture behavior of graphene. Extreme Mechanics Letters, 2015. **5**: p. 10-17.
19. Yang, G., et al., Structure of graphene and its disorders: a review. Science and technology of advanced materials, 2018. **19**(1): p. 613-648.
20. Rafiee, M.A., et al., Fracture and Fatigue in Graphene Nanocomposites. Small, 2010. **6**(2): p. 179-183.
21. Stankovich, S., et al., Graphene-based composite materials. Nature, 2006. **442**(7100): p. 282-286.
22. Sutter, P., How silicon leaves the scene. Nature Materials, 2009. **8**: p. 171.
23. Lin, Y.-M. and P. Avouris, Strong Suppression of Electrical Noise in Bilayer Graphene Nanodevices. Nano Letters, 2008. **8**(8): p. 2119-2125.
24. Abergel, D.S.L. and V.I. Fal'ko, Optical and magneto-optical far-infrared properties of bilayer graphene. Physical Review B, 2007. **75**(15): p. 155430.
25. Ohta, T., et al., Controlling the Electronic Structure of Bilayer Graphene. Science, 2006. **313**(5789): p. 951-954.
26. Jeong, G., et al., Mapping of Bernal and non-Bernal stacking domains in bilayer graphene using infrared nanoscopy. Nanoscale, 2017. **9**(12): p. 4191-4195.
27. Koshino, M. and E. McCann, Multilayer graphenes with mixed stacking structure: Interplay of Bernal and rhombohedral stacking. Physical Review B, 2013. **87**(4): p. 045420.
28. Jiao, M.D., et al., Molecular dynamics simulations on deformation and fracture of bi-layer graphene with different stacking pattern under tension. Physics Letters A, 2016. **380**(4): p. 609-613.
29. Zhang, Y.Y., et al., Mechanical properties of bilayer graphene sheets coupled by sp3 bonding. Carbon, 2011. **49**(13): p. 4511-4517.
30. Kotsilkova, R., et al., Mechanical properties investigation of bilayer graphene/poly(methyl methacrylate) thin films at macro, micro and nanoscale. Carbon, 2016. **100**: p. 355-366.
31. Rezania, H. and M. Yarmohammadi, Dynamical thermal conductivity of bilayer graphene in the presence of bias voltage. Physica E: Low-dimensional Systems and Nanostructures, 2016. **75**: p. 125-135.
32. Deshmukh, S.A., et al., The interfacial dynamics of water sandwiched between graphene sheets are governed by the slit width. Surface Science, 2013. **609**: p. 129-139.
33. Li, J. and F. Wang, Water graphene contact surface investigated by pairwise potentials from force-matching PAW-PBE with dispersion correction. The Journal of Chemical Physics, 2017. **146**(5): p. 054702.
34. Algara-Siller, G., et al., Square ice in graphene nanocapillaries. Nature, 2015. **519**: p. 443.
35. Köhler, M.H., et al., Water in nanotubes: The surface effect. Chemical Engineering Science, 2019. **203**: p. 54-67.
36. Leenaerts, O., B. Partoens, and F.M. Peeters, Water on graphene: Hydrophobicity and dipole moment using density functional theory. Physical Review B, 2009. **79**(23): p. 235440.
37. Zong, Z., et al., Direct measurement of graphene adhesion on silicon surface by intercalation of nanoparticles. Journal of Applied Physics, 2010. **107**(2): p. 026104.

38. Ribeiro, R.M., et al., Inducing energy gaps in monolayer and bilayer graphene: Local density approximation calculations. Physical Review B, 2008. **78**(7): p. 075442.
39. Rangel Cortes, E., L.F. Magaña Solís, and J.S. Arellano, Interaction of a water molecule with a graphene layer. Revista Mexicana de Física, 2013. **59**(1): p. 118-125.
40. Ma, J., et al., Adsorption and diffusion of water on graphene from first principles. Physical Review B, 2011. **84**(3): p. 033402.
41. Rafiee, J., et al., Wetting transparency of graphene. Nature Materials, 2012. **11**: p. 217.
42. Balandin, A.A., et al., Superior Thermal Conductivity of Single-Layer Graphene. Nano Letters, 2008. **8**(3): p. 902-907.
43. Alexeev, D., et al., Kapitza Resistance between Few-Layer Graphene and Water: Liquid Layering Effects. Nano Letters, 2015. **15**(9): p. 5744-5749.
44. Chialvo, A.A. and L. Vlcek, Can We Describe Graphene Confined Water Structures as Overlapping of Approaching Graphene–Water Interfacial Structures? The Journal of Physical Chemistry C, 2016. **120**(14): p. 7553-7561.
45. Neria, E., S. Fischer, and M. Karplus, Simulation of activation free energies in molecular systems. The Journal of Chemical Physics, 1996. **105**(5): p. 1902-1921.
46. Neek-Amal, M., et al., Commensurability Effects in Viscosity of Nanoconfined Water. ACS Nano, 2016. **10**(3): p. 3685-3692.
47. Hwang, J.H., et al., Local conductance mapping of water-intercalated graphene on mica. Applied Physics Letters, 2016. **109**(24): p. 241602.
48. Solanky, P., et al., The inherent behavior of graphene flakes in water: A molecular dynamics study. Computational Materials Science, 2019. **162**: p. 140-147.
49. Fermi, E., et al., STUDIES OF THE NONLINEAR PROBLEMS. 1955: United States.
50. Alder, B.J. and T.E. Wainwright, Studies in Molecular Dynamics. I. General Method. The Journal of Chemical Physics, 1959. **31**(2): p. 459-466.
51. Warshel, A., Bicycle-pedal model for the first step in the vision process. Nature, 1976. **260**(5553): p. 679-683.
52. Swope, W.C., et al., A computer simulation method for the calculation of equilibrium constants for the formation of physical clusters of molecules: Application to small water clusters. The Journal of Chemical Physics, 1982. **76**(1): p. 637-649.
53. Nosé, S., A unified formulation of the constant temperature molecular dynamics methods. The Journal of Chemical Physics, 1984. **81**(1): p. 511-519.
54. Hoover, W.G., Canonical dynamics: Equilibrium phase-space distributions. Physical Review A, 1985. **31**(3): p. 1695-1697.
55. Stuart, S.J., A.B. Tutein, and J.A. Harrison, A reactive potential for hydrocarbons with intermolecular interactions. The Journal of Chemical Physics, 2000. **112**(14): p. 6472-6486.
56. Zhang, T., et al., Flaw Insensitive Fracture in Nanocrystalline Graphene. Nano Letters, 2012. **12**(9): p. 4605-4610.
57. Yin, H., et al., Griffith Criterion for Brittle Fracture in Graphene. Nano Letters, 2015. **15**(3): p. 1918-1924.

58. Grantab, R., V.B. Shenoy, and R.S. Ruoff, Anomalous Strength Characteristics of Tilt Grain Boundaries in Graphene. Science, 2010. **330**(6006): p. 946-948.
59. Jones, J.E. and S. Chapman, On the determination of molecular fields. —II. From the equation of state of a gas. Proceedings of the Royal Society of London. Series A, Containing Papers of a Mathematical and Physical Character, 1924. **106**(738): p. 463-477.
60. Pei, Q.X., Y.W. Zhang, and V.B. Shenoy, A molecular dynamics study of the mechanical properties of hydrogen functionalized graphene. Carbon, 2010. **48**(3): p. 898-904.
61. Khare, R., et al., Coupled quantum mechanical/molecular mechanical modeling of the fracture of defective carbon nanotubes and graphene sheets. Physical Review B, 2007. **75**(7): p. 075412.
62. Jorgensen, W.L., et al., Comparison of simple potential functions for simulating liquid water. The Journal of Chemical Physics, 1983. **79**(2): p. 926-935.
63. Chen, Y., et al., Aerosol Synthesis of Cargo-Filled Graphene Nanosacks. Nano Letters, 2012. **12**(4): p. 1996-2002.
64. Bolotin, K.I., et al., Ultrahigh electron mobility in suspended graphene. Solid State Communications, 2008. **146**(9): p. 351-355.
65. Hao, F., D. Fang, and Z. Xu, Mechanical and thermal transport properties of graphene with defects. Applied Physics Letters, 2011. **99**(4): p. 041901.
66. Wei, Y., et al., The nature of strength enhancement and weakening by pentagon–heptagon defects in graphene. Nature Materials, 2012. **11**: p. 759.
67. Jin, Y. and F.G. Yuan, Nanoscopic modeling of fracture of 2D graphene systems. J Nanosci Nanotechnol, 2005. **5**(4): p. 601-8.
68. Mattoni, A., L. Colombo, and F. Cleri, Atomic Scale Origin of Crack Resistance in Brittle Fracture. Physical Review Letters, 2005. **95**(11): p. 115501.
69. Köhler, M.H., et al., Structure and dynamics of water inside hydrophobic and hydrophilic nanotubes. Physica A: Statistical Mechanics and its Applications, 2018. **490**: p. 331-337.
70. Soler-Crespo, R.A., et al., The Role of Water in Mediating Interfacial Adhesion and Shear Strength in Graphene Oxide. ACS Nano, 2018. **12**(6): p. 6089-6099.
71. Kozbial, A., et al., Understanding the intrinsic water wettability of graphite. Carbon, 2014. **74**: p. 218-225.
72. Munz, M., et al., Thickness-Dependent Hydrophobicity of Epitaxial Graphene. ACS Nano, 2015. **9**(8): p. 8401-8411.
73. Leenaerts, O., B. Partoens, and F.M. Peeters, Adsorption of H2O,NH3,CO,NO2, and NO on graphene: A first-principles study. Physical Review B, 2008. **77**(12): p. 125416.